NISTIR 6871

Monte Carlo Modeling for Intravascular Brachytherapy Sources

Stephen M. Seltzer

U.S. DEPARTMENT OF COMMERCE
Ionizing Radiation Division
National Institute of Standards
and Technology
Gaithersburg, MD 20899

NIST
National Institute of Standards and Technology
Technology Administration
U.S. Department of Commerce

NISTIR 6871

Monte Carlo Modeling for Intravascular Brachytherapy Sources

Stephen M. Seltzer

U.S. DEPARTMENT OF COMMERCE
Ionizing Radiation Division
National Institute of Standards
and Technology
Gaithersburg, MD 20899

May 2002

U.S. DEPARTMENT OF COMMERCE
Donald L. Evans, Secretary

TECHNOLOGY ADMINISTRATION
Phillip J. Bond, Under Secretary for Technology

NATIONAL INSTITUTE OF STANDARDS
AND TECHNOLOGY
Arden L. Bement, Jr., Director

Monte Carlo Modeling for Intravascular Brachytherapy Sources

Stephen M. Seltzer

Ionizing Radiation Division
National Institute of Standards and Technology
Gaithersburg, MD 20899

1. Introduction

Monte Carlo codes for the solution of coupled electron-photon transport problems have been undergoing development and refinement for the last 40 years, roughly in parallel with the advancement of computing technology. In general mathematical terms, the Monte Carlo method provides a solution to the integro-differential Boltzman equation that governs radiation transport. The transport equation generally involves six or more variables[1]. Formal solutions to the transport equation have been developed only in rather restrictive approximations, usually disregarding one or more of the variables. While not sufficient by themselves for general transport problems, these limited solutions, particularly those for electron transport, provide the basis for many of the Monte Carlo methods in use today. A number of these partial results, mainly for relatively short pathlengths, will be alluded to in later discussion. Perhaps noteworthy as an exception to the previous remark is the moment-method solution of Lewis (1950) and Spencer (1955, 1959) for the spatial distribution of absorbed dose from an electron completely slowing down, but which ignores energy-loss fluctuations and is limited to an unbounded, homogeneous medium.

With the availability of more powerful computers, codes for the numerical integration of the transport equation have been developed for electron-photon transport, based on the discreet-ordinates, or S_n, method used for neutron transport. Morel, Lorence and their collegues (Morel,1979; Morel and Wienke, 1982; Lorence, Nelson, and Morel, 1985; Lorence, Morel, and Valdez, 1989a, 1989b, 1990; Lorence, 1992; Lorence and Morel, 1992) developed a reasonably successful one-dimensional calculation involving complex numerical procedures using carefully prepared scattering matrices. Work on multi-dimensional treatments is reported by Fillipone *et al.* (1990), Datta, Ray, and Wienke (1992), Datta *et al.* (1992), Datta and Ray (1993), and Drumm (1997). These deterministic calculations have the advantage of producing results free of statistical fluctuations, but are subject to approximations used in the calculations and to some numerical artifacts. There appear to be few successful applications of discrete-ordinates methods to medical physics applications. Daskalov *et al.* (2000a, 2000b) recently reported pilot calculations for photon-emitting brachytherapy sources using the DANTSYS two-dimensional discrete-ordinates code. Although required accuracy seems attainable, at least for photon sources and with computational fine-tuning, the computing time for discrete-ordinates calculations in two or three dimensions approaches that for Monte Carlo calculations.

[1] The time dependence is usually not of interest in our applications. The type of particle (secondary knock-on electron, bremsstrahlung photon, etc.) while formally perhaps not a variable nonetheless adds an additional dimension.

The Monte Carlo method, while making no direct explicit use of the transport equation, evaluates the integral by statistical sampling. This is done by imitating the transport of the radiation, *i.e.*, letting the particles carry out a random walk, with probabilities for the various interactions and outcomes governed by our knowledge of the pertinent cross sections. Random walks, or histories, are repeated numerous times until the desired result is obtained with some level of useable statistical accuracy. The disadvantage of this method, other than the significant amount of computer time required, is the statistical nature of the calculated histogram distributions (the New York skyline) and the associated difficulty in isolating and understanding small effects. Its great advantage lies in the inherent ability of Monte Carlo calculations to handle any source or boundary conditions. The development of a Monte Carlo code is thus largely intuitive rather than mathematically complex, but does require the inclusion of all the radiation physics we know and suitable approximations for what we don't.

Some interesting historical background and views on electron-photon Monte Carlo is offered by Nahum (1988) and by Bielajew (2001), from the perspective of medical physicists; see also a good review by Andreo (1991). Those in this field unequivocally credit Berger's (1963) seminal work as the "bible" for charged-particle Monte Carlo methods, both because it cogently laid out in rather complete detail all the components involved in these calculations and because it is remarkably current still today. Applications of electron-photon Monte Carlo calculations to medical physics seem to have begun in earnest after about 1980, when codes attained more geometrical generality and user friendliness, and were publicly distributed. Now Monte Carlo calculations have become increasingly recognized as useful and accurate tools in medical physics, providing a valuable adjunct to measurement.

With the advent of intravascular brachytherapy (IVBT) about 10 years ago, it is logical for Monte Carlo calculations to have been applied to the important, and experimentally difficult, dosimetry characterization for these sources. Fox (2002) has published a nice review of IVBT, including a rather thorough review of the theoretical dosimetry applied for these sources. This presentation will attempt to review the application of general-purpose, public-domain Monte Carlo codes to IVBT. These include the Integrated Tiger Series (ITS), the MCNP series, and the EGS series. I will include some comments on the more recent PENELOPE code, although I am not aware any reports on its use for IVBT. In what follows, some background will be presented on the basic Monte Carlo models and cross-section information used by the codes to help in their characterization. Second, Monte Carlo results for IVBT application will be reviewed and, where possible, compared. Finally, a fast but approximate calculation using point kernels will be outlined and discussed.

2. Monte Carlo Models

Although somewhat general, the discussion here pertains mainly to those general-purpose, coupled electron-photon Monte Carlo codes[2] that treat radiation transport from, say, 100 Mev or higher, down to about 1 keV, *i.e.*, covering the energy range of interest in radiation therapy. These codes consist of a few ingredients: (a) the Monte Carlo model and sampling algorithms, (b) the underlying radiation-interaction cross sections and multiple-scattering distributions,

[2] There are of course a number of other codes that have been developed, *e.g.*, electron single-scatter codes to very low energies to calculate electron track structures for radiobiological applications.

(c) tracking algorithms to determine when boundaries have been crossed during a step in the random walk, and (d) a good random-number generator. Considerable effort has been expended in developing and refining these ingredients, particularly (a) and (b), above. A brief and partial chronicle[3] of the development of the codes under consideration in this work is indicated in figure 1. The GEANT code (Brun *et al.*, 1986) will not be discussed here; it is a widely used high-energy code, with a few applications to IVBT reported, but I am far less familiar with it than with the others.

In all of these codes, the transport of photons is done by analog Monte Carlo routines: photon trajectories are generated in complete analogy with the physical process, that is, following photons from interaction-to-interaction using the relevant single-interaction cross sections. The main differences among codes should mainly be a consequence of the basic photon-interaction cross sections used. There can be of course other higher order differences (*e.g.*, handling of binding effects for the incoherently scattered photon), but these should be relatively unimportant in applications to IVBT.

Electron (and positron) transport in principle can be done completely also in a single-scattering treatment. However, the number of collisions, both elastic and inelastic, experienced by MeV electrons in the course of slowing down is very large due to the long range of the Coulomb interaction between the charged particle and the atoms comprising the medium. With the availability of extremely fast computers, the large numbers of collisions that would need to be simulated is perhaps not the obstacle it once was. Rather complete and accurate information is available on the cross section, differential in scattering angle, for the *elastic* scattering of electrons and positrons by neutral atoms (see, *e.g.*, Berger and Seltzer, 2000). However, a single-scattering treatment requires more detailed information than is generally known on the differential electron-atom *inelastic*-scattering cross section, but which is subsumed in the much-more readily available stopping powers. Thus, these Monte Carlo codes use "condensed" histories, or random walks comprised of path segments for which the effects of multiple scattering are sampled. Berger (1963) rather thoroughly outlined the condensed charged-particle history methods, including the pertinent multiple-scattering distributions. Berger separated the schemes into two classes. Class I is a complete-grouping algorithm in which *all* energy losses and all elastic-scattering events occurring in a pathlength are sampled from multiple-scattering distributions. Class II is a mixed-procedure algorithm in which the relatively infrequent energy losses greater than some cut-off ("catastrophic") are treated as single interactions, and the smaller more numerous energy losses are assumed governed by the average energy loss for the sampled pathlength to the catastrophic collision.

I will try to outline some of the basic features of the general-purpose Monte Carlo codes, but I am aware that my limited knowledge might result in some inaccuracies and omissions. The reader should consult the pertinent references or the code developers and expert users.

[3] My understanding of the history and the particular features in each code and its versions is no doubt imperfect. I apologize in advance to the code developers and to anyone else who knows better.

2.1 ETRAN

Referring again to figure 1, the first version of ETRAN (Berger and Seltzer, 1968) grew out of Berger's 1963 outline. The code handled only a homogeneous medium[4] in a Class I scheme incorporating physics designed for accuracy in the energy region from, say, 10s of MeV down to some 10s of keV. The net deflection angle from multiple elastic scattering in a path segment was sampled from the Goudsmit-Saunderson (1940) distribution, which is exact for any assumed single-scattering cross section (*i.e.*, not derived in the small-angle approximation). The single-elastic-scattering cross section was taken as the Rutherford cross section, corrected for screening effects using a parameter from the work of Molière (1948), and corrected for spin and relativistic effects using the results of Mott (1929). The mean energy loss by electrons and positrons in a path segment was taken from then-current stopping powers (Berger and Seltzer, 1964, 1966). Fluctuations about the mean energy loss were sampled from the Landau (1944) distribution, with modifications suggested by Blunck and Leisegang (1950). Electron-bremsstrahlung production and energy loss were calculated from analytical Bethe-Heitler theory (Koch and Motz, 1959), soon to be adjusted by improved empirical corrections (Berger and Seltzer, 1970). The production of knock-on electrons with energies greater than a chosen cut-off was sampled from the Møller (1932) or Bhabha[5] (1936) cross sections, consistent with the calculation of the collision stopping power. Photon-interaction cross sections were taken from the work of Hubbell (1969). The complete electron-photon cascade could be followed down to 1 keV.

Improvements were incorporated over the years: new photon-interaction cross sections (Hubbell, 1982; Berger and Hubbell, 1987); new electron and positron stopping powers (Berger and Seltzer, 1982; ICRU, 1984); new bremsstrahlung-production cross sections (Seltzer and Berger, 1985, 1986); corrections to energy-loss straggling sampling (Seltzer, 1988); and a pathlength wiggliness (spatial-displacement) correction (Seltzer, 1991). Seltzer (1988, 1991) provides a fairly complete summary of the basis and algorithms used in ETRAN.

2.2 Integrated Tiger Series (ITS)

ETRAN provided the physics engine for the coupled electron-photon codes developed at the Sandia National Laboratories, which evolved to include a variety of geometrical, multi-material capabilities. The SANDYL early code (Colbert, 1974) included a combinatorial-geometry package for complete generality, but was not maintained. Independently, Halbleib and co-workers developed a series of codes including the one-dimensional, multi-slab TIGER code (Halbleib and Vandevender, 1975), the cylindrical-symmetry, three-dimensional, multi-material CYLTRAN code (Halbleib and Vandevender, 1976), and the general combinatorial-geometry, three-dimensional, multi-material ACCEPT code (Halbleib, 1980). A more complete treatment of atomic relaxation following ionization was added (Halbleib and Morel, 1979), as well as the effects on electron transport of applied macroscopic electric and magnetic fields (Halbleib and Vandevender, 1977). The calculation of multiple-elastic-scattering distributions was updated (Haggmark, MacCallum, and Riley, 1974) to include the exact, phase-shift results for the differential cross section from Riley's calculations (Riley, MacCallum, and Biggs. 1975) for

[4] Various versions handled slab, cylindrical or spherical targets.

[5] This was not implemented in public-domain versions, and knock-on electrons from positrons were sampled as if produced by electrons.

electron energies below 256 keV, improving on the use of the Rutherford cross section with Molière screening and Mott spin and relativistic corrections.

The separate codes for handling various geometries and effects were organized into the **I**ntegrated **T**iger **S**eries (ITS) (Halbleib and Mehlhorn, 1984, 1986; Halbleib, 1988) to facilitate updating of the entire suite. Various improvements in ETRAN have been incorporated into the ITS (see figure 1), resulting in version 3 (Halbleib *et al.*, 1992a, 1992b) now current for the last decade. One point should be noted here: ITS does not have an option to sample from a uniform emitting volume, crucial to the modeling of IVBT sources. I had to create a patch to accomplish such sampling for the work described here.

2.3 MCNP

The **M**onte **C**arlo **N**-**P**article (MCNP) transport code has a long history as a Monte Carlo code for the transport of neutrons and photons. Version 4 of the MCNP code was expanded to include electron transport, incorporating algorithms and data from ITS version 1 (Briesmeister, 1993) and issued as MCNP4A. This treatment was based on the older 1964 electron and positron stopping powers and bremsstrahlung-production cross sections. It was later updated to include the ITS 3 use of the newer stopping powers and bremsstrahlung cross sections, becoming MCNP4B (Briesmeister, 1997). The current version is MCNP4C (Briesmeister, 2000; Hendricks *et al.*, 2000). MCNP does include the relevant sampling for an emitting volume.

The electron transport physics is mainly from the relevant version of the ITS code. Some differences arise in implementation, notably involving energy-grid indexing (to locate the pertinent multiple scattering distributions) and schemes to tally various results. Note that photon-interaction cross sections appear (Hendricks, Frankle, and Court, 1994) to be derived from Storm and Israel (1967), using the Evaluated Photon Data Library (Cullen, Perkins, and Rathkopf, 1990) to extend coverage from 100 MeV to 100 GeV.

2.4 EGS

The Electron Gamma Shower (EGS) code is based on a Class II scheme, and grew out of efforts to improve and generalize the Monte Carlo treatment by Nagel (Nagel and Schlier, 1963; Nagel, 1965) of high-energy showers initiated by electrons in lead. By 1974, the various versions developed at the Stanford Linear Accelerator Center evolved into EGS1. This code treated showers in a homogeneous medium from 1000 MeV down to electron kinetic energies of 1 MeV and photon energies down to 0.25 MeV, using somewhat crude discrete transport algorithms, and incorporating the photon-interaction cross sections of Storm and Israel (1970). The 1975 EGS2 version was expanded to include multiple materials, with the geometry specification and scoring algorithms moved to user-written routines. The EGS3 code system (Ford and Nelson, 1978) incorporated a number of improvements, including the transport of electrons and photons in random rather than discrete steps. The electron transport is based on Molière's theory (1947, 1948) of multiple-elastic scattering, derived in the small-angle approximation. In EGS3, the sampling of the net multiple-scattering deflection angle was extended to a continuous rather than discrete distribution. The energy region handled by the code was extended upwards to then treat

showers from 100 GeV, down still to 1 MeV for electron or positron kinetic energy and now 0.1 MeV for photons.

Improvements in electron and photon transport led to the 1985 EGS4 version (Nelson, Hirayama, and Rogers, 1985). The energy range treated now extended from several thousand GeV down to ~10 keV[6] for electron and positron kinetic energy and 1 keV for photons. Other improvements accumulated, notably including the spatial-displacement corrections provided by PRESTA (Bielajew and Rogers, 1986, 1987, 1988); the introduction of continuous bremsstrahlung-production angular distributions (Bielajew, Mohan, and Chui, 1989); and the use of ICRU (1984) stopping powers (Duane, Bielajew, and Rogers, 1989; Rogers *et al.*, 1989).

The recent successor version, EGSnrc (Kawrakow, 2000) revamped a significant portion of the physics. Through the work of Kawrakow and Bielajew (1998), the Goudsmit-Saunderson formulation of the multiple-elastic-scattering distribution was incorporated into the Class II Monte Carlo model, replacing the inferior Molière theory. This algorithm appears to be based on the use of the Rutherford single-scattering cross section with Molière screening and Mott spin and relativistic corrections. Notable among other changes is the incorporation of a much improved algorithm for including spatial-displacement corrections, and options to implement the simulation of atomic relaxation following photon-ionization events, the selection of bound- or free-electron Compton scattering, and the selection of the Seltzer-Berger bremsstrahlung-production cross sections.

2.5 PENELOPE

The development of the PENELOPE (**PEN**etration and **E**nergy **LO**ss of **P**ositrons and **E**lectrons) code began in the early 1990s. The current version (Salvat *et al.*, 2001) treats the electron-photon cascade from 1 GeV down to 0.1 keV. It is based on Class II algorithms for the charged particles that treat hard collisions, both for elastic scattering angles and for energy losses larger than chosen cutoffs, as single interactions, and the soft collisions through multiple-scattering distributions. In the current version, single- and multiple-scattering angular deflections are sampled from distributions based on the use of plausible analytical forms of the differential scattering cross section whose parameters are fitted to the zeroth, first and second moments (of the deflection cosine) of exact, phase-shift results. Energy loss is based on an inelastic-scattering model in which the generalized oscillator strength for distant (soft) collisions is represented by a series of simple oscillators such that the result for the aggregate satisfies appropriate sum rules and includes the density effect, and the close (hard) collisions are assumed governed by the Møller or Bhabha cross sections for electrons and positrons, respectively. Bremsstrahlung-production cross sections and radiative stopping powers are from Seltzer and Berger (1985, 1986).

Photon-interaction cross sections are derived from a number of sources. The total cross sections for photoelectric-absorption are taken from Cullen, Hubbell, Kissel (1997), pair and triplet production from Hubbell, Gimm, and Øverbø (1980). Cross sections for coherent scattering are based on analytical fits to the non-relativistic atomic form factors of Hubbell *et al.* (1975). Incoherent scattering is treated in an impulse approximation based on analytical fits to Compton

[6] It is possible to follow electrons and positrons down to a kinetic energy of 1 keV.

profiles of Biggs, Mendelsohn, and Mann (1975). For the simulation of atomic relaxation following ionization-produced vacancies in the K and L shells, the transition probabilities of Perkins *et al.* (1991) are used.

3 Photon Monte Carlo in IVBT Dosimetry

3.1 Some Discussion of Cross Sections

Although photon transport is of secondary importance for the pure beta emitters used and considered for IVBT (*e.g.*, $^{90}Sr/^{90}Y$, ^{90}Y, ^{32}P), it is of course of primary importance for the (effectively) pure photon emitters (*e.g.*, ^{192}Ir, ^{125}I, perhaps ^{103}Pd) and of some significance for mixed beta/photon emitters (*e.g.*, $^{188}W/^{188}Re$, ^{188}Re). Because of the sensitivity of dose calculations to the assumed photon-interaction cross sections, the Low-Energy Interstitial Brachytherapy Dosimetry Subcommittee of the AAPM is recommending that the photon cross-section data set be clearly identified when reporting calculated results for ^{125}I and ^{103}Pd sources.

For reference, cross sections for photon interactions in water, the standard phantom material in these applications, are shown in figure 2. The data, cast as partial and total attenuation coefficients, are from the XCOM database of Berger and Hubbell (1987). The interaction processes include: photoelectric absorption in which the all of the energy of the incoming photon is lost and an atomic electron is ejected; incoherent scattering in which a portion of the energy of the incoming photon is lost, and its direction is changed, in the transfer of momentum to an atomic electron; coherent (Rayleigh) scattering in which the photon energy is essentially unchanged, but its direction is changed; pair production in the field of the atomic nucleus in which the photon energy is converted to that of an electron-positron pair; and triplet production in the field of the atomic electrons in which the energy is converted to that of an electron-positron pair and an ejected atomic electron. In water at photon energies below ~30 keV, photoelectric absorption dominates; at energies greater than ~30 keV incoherent scattering dominates, up until ~30 MeV where pair production begins to dominate.

Related to the photon mass attenuation coefficient are the photon mass energy-transfer coefficient and the photon mass energy-absorption coefficient. The energy-transfer coefficient is the mean fraction of the photon energy initially converted to kinetic energy of secondary charged particles, per unit tracklength. The energy-absorption coefficient further discounts the energy transfer by the amount of energy converted back to photons through radiative processes in the course of the secondary electrons slowing down. These coefficients can be used to convert the spectrum of photon fluence to kerma and to absorbed dose, respectively, under conditions of charged-particle equilibrium, by integrating over energy the product of the photon fluence spectrum, photon energy and the relevant coefficient. The mass energy-absorption coefficient for water, from Seltzer (1993), is plotted along with the total attenuation coefficient in figure 3. For water in this energy range, the energy-transfer and energy-absorption coefficients are nearly identical. The ratios of the photon mass energy-absorption coefficient from older tabulations to those of Seltzer (1993) are shown for water in figure 4. It is not clear how relevant these comparisons are to Monte Carlo dosimetry calculations for photon brachytherapy. Monte Carlo codes can calculate the energy deposited in scoring regions by tracking the secondary photons and electrons as they lose energy, and/or they can calculate the spectrum of photon fluence in

scoring regions. The former essentially invokes the photon energy-transfer mechanisms and data built into the Monte Carlo algorithms, while use of the latter assumes charged-particle equilibrium and requires an integral, performed either during the generation of histories in the code or after the final fluence spectra are tallied. It appears to be the more usual practice to directly score the energy deposited (*e.g.*, using the *f8 tally in MCNP) so that use of the mass energy-absorption coefficient is relatively infrequent in these applications. The energy-absorption coefficient is, however, integral to classical point-kernel implementations, to be discussed later.

DeMarco, Boedeker, and Wallace (2002) have elucidated the choice of photon-interaction data by identifying the photon cross sections used in some of the major Monte Carlo codes, comparing the cross sections, and determining the magnitude of the differences using them in a set of dose calculations with the MCNP4C code. A somewhat similar comparison of the basic cross sections is shown in figure 5, where ratios of the total attenuation coefficient (including coherent scattering) to that from the XCOM database is plotted for water. The use of XCOM data as the reference is not necessarily meant to imply that it is the most accurate, but it is a well-known database, it is easily available[7], and its use follows the lead of DeMarco *et al.* There is agreement to ~1% above 100 keV, but differences as large as 3% to 5% in the 20 keV to 40 keV region. The ~3% excess in the EGS4 total attenuation coefficient at 30 keV to 40 keV would seem to be due to the use of the cross section for Compton scattering from free rather than from bound atomic electrons.

The effects of these differences on the calculated spatial distribution of absorbed dose from brachytherapy sources are best determined using the same Monte Carlo code. DeMarco *et al.* compare the absorbed dose at 1 cm in water from point sources using various cross-section data sets in MCNP4C. They find absorbed-dose differences to be as much as ~7% lower in the region of photon energies from 20 keV to 40 keV using Storm and Israel (1967) rather than XCOM cross sections. Interestingly they find differences of 2% to 3% (in the same direction) when they superimpose the EGS4 results of Luxton and Jozseph (1999). This relative success is perhaps explained by the fact that the excess of the Compton scattering cross section from free electrons is at forward angles with little energy loss, thus nearly mimicking no scattering, which approximates the reduction of the scattering cross sections when binding effects are included.

Noting that encapsulation materials for brachytherapy sources are often Ti, Ni-Ti alloys and steel, we plot the ratios of the total attenuation coefficient (including coherent scattering) to that from XCOM for Fe in figure 6. The differences are usually in the 1% to 2% range (the stated accuracy of the EGS fits to photon cross-section data), except for the Storm and Israel (1967) data (the default set in MCNP4) near 20 keV where the difference is ~3%.

3.2 Some Pertinent Monte Carlo Literature

There have been a number of early Monte Carlo studies for photon-emitting brachytherapy sources that were done to calculate the dose rate mainly at distances in water of 1 cm and larger. Williamson (1991) used his MCPT[8] code to calculate dose rates in water for ^{125}I and ^{192}Ir seeds,

[7] See the web site http://physics.nist.gov/PhysRefData/contents.html.

[8] Williamson's (1988) Monte Carlo Photon-Transport (MCPT) code simulates only photon transport.

and more recently Daskalov, Löffler, and Williamson (1998) employed it to calculate the dose-rate distribution for a new HDR ^{192}Ir source at distances down to 1 mm. Ballester *et al.* (1997) used the GEANT3 code to calculate dose-rate distributions in water around ^{192}Ir wire sources, at distances down to 1.5 mm. These calculations were repeated by Pérez-Calatayud *et al.* (1999) and by Ballester *et al.* (2001) for other ^{192}Ir sources. Mason *et al.* (1992) and MacPherson and Battista (1995) used MCNP4A to calculate the dosimetric parameters of ^{169}Yb sources. Wallace, Wong, and Fernando (1998) used MCNP4A in their dosimetric studies of HDR ^{192}Ir sources. Wierzbeicki *et al.* (1998) used MCNP to calculate the dose-rate distribution for a ^{125}I source. Cho, Muller-Runkel, and Hanson (1999) used only the photon transport in MCNP4A in their calculations for an HDR ^{192}Ir source; and Baltas *et al.* (2001) report results for the radial dose-rate distributions from MCNP4B calculations for a number of HDR ^{192}Ir sources.

Thomason *et al.* (1991) used EGS4 to calculate the radial dose-rate distribution from ^{192}Ir and ^{137}Cs seeds in water. EGS4 was used also by Rashid *et al.* (1992) to calculate the radial dose-rate distribution from a point source of ^{125}I, both in water and in polystyrene to test scaling. Wang and Sloboda (1996) calculated the distributions of absorbed dose in water from ^{125}I, ^{169}Yb and ^{192}Ir brachytherapy sources using a version of EGS4 in which binding corrections to Compton scattering and K-shell fluorescence were incorporated. Wang and Sloboda (1998a, 1998b) used EGS4 to calculate the dose-rate distribution in water at radial distances down to 1 mm for a number of ^{192}Ir brachytherapy sources. In these cases, the photon fluence spectra were tallied, and the mass energy-absorption coefficients of Hubbell (1982) were used to convert to absorbed dose. Using essentially the XCOM photon-interaction cross sections (DLC-136/PHOTX[9]) in EGS4, Mainegra, Capote, and López (2000) calculated the radial dose functions for ^{103}Pd, ^{125}I, ^{169}Yb and ^{192}Ir brachytherapy sources at distances down to 5 mm.

For applications explicitly to IVBT, Wang and Li (2000) used EGS4 to calculate dose-rate distribution in water and solid water for the Best Industries ^{192}Ir seed. Reynaert *et al.* (2001) also used EGS4 in their dosimetry calculations for the Cordis ^{192}Ir seed sources. Li (2001) employed EGSnrc to study the dose perturbations due to contrast media for the Best Industries ^{192}Ir seed. Baltas *et al.* (2001) used their own photon Monte Carlo code and MCNP4B to investigate both the gamma and beta components of the dose rate close to ^{192}Ir sources. Stabin *et al.* (2000) used the average of their results from MCNP4B and EGS4 calculations to determine the dose-rate distributions for ^{192}Ir wire sources and for ^{186}Re and ^{188}Re balloon sources, with and without the presence of high-density plaque.

4 Electron Monte Carlo in IVBT Dosimetry

4.2 Some Remarks on Model Effects

Differences among electron-transport results from the various Monte Carlo codes can arise for a number of reasons, perhaps more in number and in complexity than in photon transport. As for photons, one can look at the underlying cross-section information, *e.g.*, collision and radiative energy losses and multiple-elastic-scattering angular distributions, but for electrons the choices of cutoffs and step sizes and the way the processes are handled in boundary-crossing algorithms

[9] This is the designation given by the Radiation Safety Information Computational Center (RSICC), Oak Ridge National Laboratory. See their web site at http://www-rsicc.ornl.gov/rsic.html.

also become important. Wang, Li, and Yu (2000) investigated this issue for EGS4 applied to the Novoste $^{90}Sr/^{90}Y$ seed. Schaart *et al.* (2002a) has looked into similar effects for the MCNP4C code applied to beta dosimetry in general and found that there can be significant effects, for which they propose an improved algorithm. Wang and Li (2001a) compared for the Novoste $^{90}Sr/^{90}Y$ seed the radial dose-rate distributions calculated with EGS4, EGSnrc and MCNP4B, finding agreement to within 2% at the reference radius of 2 mm but increasingly poorer agreement at larger distances (as much as 20% at 5mm to 6 mm). Wang and Li (2001b) then modeled the Guidant 27 mm ^{32}P source with EGSnrc, opting (as in their earlier tests) for the single-elastic scattering boundary-crossing algorithm, the PRESTA-II electron-step algorithm, and the use of single-elastic-scattering cross sections with relativistic and spin corrections. They also calculated the radial dose-rate distribution with EGS4 and compared their results with MCNP4B2 results of Mourtada *et al.* (2000). They found that although the three results agreed at a radial distance of 1 mm, EGS4 was ~1.5% lower than EGSnrc and MCNP4B2 ~2% higher at 2 mm, and at 4 mm EGS4 was ~7% lower and MNCP4B2 was ~6% higher.

There would seem to be no issue pertaining to the choice of collision and radiative stopping powers, as the current codes indicate they use by convention the data from Report 37 of the International Commission on Radiation Units and Measurements (ICRU, 1984). This would seem to be the case, except perhaps in our recent use of the PENELOPE code. PENELOPE uses a model for the collision-energy-loss spectrum whose mean should give the Bethe-theory result at sufficiently high energies (say $\geq$10 keV for low-Z materials), including the density-effect correction. When we set up a PENELOPE pre-processing run using default parameters, a choice of considering the material in question either as a conductor or as an insulator was initially overlooked. For condensed media, this is an important choice in the calculation of the density-effect correction. Figure 7 shows, for liquid water with a mean excitation energy of 75 eV, the ratio of the collision stopping power calculated by PENELOPE both as a conductor and as an insulator to that from ICRU Report 37, which treats water as an insulator. As an insulator in PENELOPE the agreement is very good. As a conductor, the PENELOPE values are low by as much as 3% at energies around 1 MeV, energies typical of the beta emitters used in IVBT. The effect of making the wrong choice will be illustrated later by Monte Carlo results for a test problem.

4.2 Some Additional Pertinent Monte Carlo Literature

Soares *et al.* (1998) included results of ITS1 calculations (using the CYLTRAN module) for the early Novoste $^{90}Sr/^{90}Y$ seed in an A-150 phantom for comparison with measured data. As in the study for the ^{192}Ir seed, Li (2001) used EGSnrc to study for the Novoste source the modification of the dose-rate distribution by the contrast media. Earlier for the Novoste $^{90}Sr/^{90}Y$ source, Ye *et al.* (2000) had used MCNP4B to quantify dose perturbations due to the presence of metallic stents, while Li *et al.* (2000) used EGS4 to calculate the dosimetric effects due both to metallic stents and to calcified plaque. Baltas *et al.* (2001) report results of their MCNP4B calculations for the Novoste $^{90}Sr/^{90}Y$ source, as well as for the beta component of ^{192}Ir HDR sources.

Todorovic *et al.* (2000) used MCNP4B and EGS4 in their calculations of the spectrum and the absorbed dose as a function of depth in polymethyl methacrylate (PMMA) for the Novoste $^{90}Sr/^{90}Y$ source and the Guidant 27 mm ^{32}P source. Sehgal *et al.* (2001) used MCNP4B to study

the dosimetric effects of source centering and calcified plaque for both the Novoste $^{90}Sr/^{90}Y$ source and the Guidant 27 mm ^{32}P source. Li and Shih (2001) used EGS4 to look at the dose effects caused by the guide wire for these sources. Mourtada *et al.* (2000) reported results of MCNP4B2 calculations of the radial dose-rate distribution in water and in A-150 plastic for the Guidant 27 mm ^{32}P source to compare with measurements. These authors also show good agreement between results from MCNP4B2 and from ITS3 (CYLTRAN module) for the factor to convert the absorbed-dose rate in A-150 to that in water. Bohm, Mourtada, and Das (2001) performed dosimetry measurements and calculations for the same Guidant 27 mm ^{32}P source, using both the MCNP4B2 and the MCNP4C Monte Carlo codes. They found slightly higher dose rates with version 4C, by about 1%.

Häfeli *et al.* (2000) report on dosimetry measurements of a prototype 40 mm $^{188}W/^{188}Re$ source, including some results from their own Monte Carlo code described as similar to EGS4 but done in the continuous-slowing-down approximation (*i.e.*, without energy-loss fluctuations). Clarijs *et al.* (2000) model the same prototype source (from Nucletron) using EGS4 to obtain the radial dose-rate distributions in water and in PMMA. Recently Schaart *et al.* (2002b) used their modified MCNP4C code (Schaart *et al.*, 2002a) to calculate the radial dose-rate distribution in PMMA for this Nucletron prototype source. They find good agreement with measurement and with the earlier EGS4 results of Clarijs *et al.* (2000) out to ~ 4 mm, beyond which the EGS4 results fall off too rapidly. Schaart (2002) continues the use of his modified MCNP4C code to model the source in water and in PMMA in his investigation of scaling the dose distribution from one medium to another for finite-diameter beta line sources.

Reports of Monte Carlo calculations of the dose-rate distributions around radioactive stents include those of Li *et al.* (1998) using MCMP4A for the positron emitter ^{48}V, and of Reynaert *et al.* (1999) using EGS4 for ^{32}P and ^{198}Au.

4.3 A Few Unpublished NIST Monte Carlo Results

Early in the development of measurement methods to support dosimetry measurement standards for beta-emitting IVBT sources, calculations were done at the National Institute of Standards and Technology (NIST) using the CYLTRAN module of ITS3 to better understand the issues. In this case, a simple patch was added to CYLTRAN to simulate a uniform cylindrical volume of isotropic emission in modeling the source. In 1997 our concern was with the Novoste $^{90}Sr/^{90}Y$ seed source and the NeoCardia (to become the Guidant) 27 mm ^{32}P "wire" source. For the Novoste source the single seed (2.5 mm in length) was modeled as a ceramic core (2.3 mm long x 0.54 mm diameter) and stainless steel encapsulation (OD of 0.64 mm and end plates 0.1mm thick). The dose-rate distribution around the seed was calculated in water and in A-150 plastic (used as the phantom material for our radiochromic film measurements) in 0.1 mm (axial) x 0.1 mm (radial) scoring bins. Figure 8a shows the calculated radial dose-rate distributions in the perpendicular bisecting plane of the seed axis. The distributions could be suitably superimposed to mimic the radial dose-rate distribution from a 12-seed train, with these results shown in figure 8b. By fitting the fine histogram data [in $\log(r^2\dot{D})$ vs. r] using least-squares cublic splines, smooth curves could be plotted. These results are summarized in figure 9. Important here is that these data could be used to correct the result measured at a distance of 1.98 mm in A-150 plastic

to that corresponding to the reference distance of 2 mm in water as prescribed by Nath *et al.* (1999).

Similar calculations were done for the Guidant 27 mm ^{32}P wire source. The wire was modeled as concentric cylinders: basically as a 27 mm long cylinder of rayon 0.203 mm in diameter, surrounded by a 0.019 mm thick annulus of polyimide, surrounded by a 0.032 mm thick annulus of air, surrounded by a 0.076 mm thick annulus of nitinol (Ni-Ti alloy). Top and bottom nitinol disks, 1.3 mm thick and 0.457 mm in diameter, completed the encapsulation of the above assembly, which was then surrounded by a 0.089 mm thick annulus of water, surrounded by a 0.127 mm thick annulus of catheter, and then placed in the assumed phantom material. Figure 10 compares the intrinsic beta emission spectrum and the spectrum emerging from the nitinol walls. The calculated radial dose-rate distributions for the source-in-catheter, both in water and in A-150, are shown in figure 11.

Although comparisons of results from various Monte Carlo calculations for an IVBT source have been reported (see, *e.g.*, Wang and Li, 2001a, 2001b), it was a goal of this presentation to do a well-controlled comparison, in this case, for the new Guidant 20 mm ^{32}P source. For this exercise the wire was modeled rather similarly to the earlier Guidant wire, but with an active length of only 20 mm. A CYLTRAN/ITS3 calculation had been done for this source based on 10M primary histories, sampled from a 100-bin histogram representing the ^{32}P emission spectrum, and following electrons and photons down to cutoff energies of 1 keV. In this calculation the default electron step sizes were used, and the scoring regions in the water phantom were annuli with both radial thickness and axial thickness of 0.1 mm. The geometry and the material composition are listed in tables 1 and 2. Note that in CYLTRAN energy is deposited in these scoring regions without invoking boundary crossings (done only for crossing real material boundaries). For the other Monte Carlo codes tested, entering and leaving the scoring volumes entails boundary crossings. To keep the crossings to a minimum for these codes, the scoring regions were defined as annuli of radial thickness 0.1 mm and axial length 15 mm, centered along the active wire length. The CYLTRAN results were collapsed to correspond to the same scoring volumes, observing that the radial distribution is effectively constant over this axial length, and the statistical uncertainties of the results are greatly reduced with such averaging. The current versions of MCNP4C, EGS4, EGSnrc and PENELOPE were run for the same case, based on 10M primary histories, using the same 100-bin source spectrum, the same cutoff energies, the same material compositions and dimensions, and the default values for electron step sizes and other transport parameters. For EGS4 and EGSnrc, some of the materials are not in their database, so electron collision-stopping-power density-effect corrections were calculated as done for ICRU Report 37 and read into their cross-section generating modules. The resultant radial dose-rate distributions are shown in figure 12. Differences are difficult to discern on these logorithmic plots. Instead, the ratios of the radial dose-rate distributions to that from CYLTRAN are plotted in figure 13. The EGSnrc and EGS4 results seem nearly the same as each other but fall to ~5% lower than those of CYLTRAN at a radial distance of 4 mm, and the MCNP4C results rise to ~7% higher than those of CYLTRAN at 3 mm to 4 mm. Wang and Li (2001b) found a somewhat different relation between results from EGS4 and from EGSnrc for the Guidant 27 mm ^{32}P source, but a similar difference between the MCNP4B2 results of Mourtada *et al.* (2000) and those of EGS4. A summary of Monte Carlo results for the dose rate at radial distances of 2 mm and 4 mm is given in table 3. The Monte

Carlo results show a spread of ~6% at 2 mm and about 20% at 4 mm. Because of the error in the density-effect correction made in setting up one of the PENELOPE runs, those results cannot be considered on the same footing as the others, but rather to illustrate what can perhaps go wrong when non-experts choose default parameters.

5 Point-Kernel Calculations

Methods to calculate the spatial distribution of absorbed dose in a homogeneous medium from point sources of photons and beta particles emitted by radioactive atoms have been investigated for more than 50 y. The isotropic source produces a spherically symmetric absorbed-dose distribution that is a function of a single spatial variable r, the distance from the point source. This quantity has been of great interest in nuclear medicine. When given in terms of the fraction of the emitted energy that is absorbed per unit mass of the medium, this absorbed-dose distribution is known as the point-isotropic specific absorbed fraction or the point kernel[10] (see Loevinger and Berman, 1968). The absorbed-dose rate at distance r from the source is

$$\dot{D}(r) = A k n E \Phi(r), \tag{1}$$

where here A is the source activity in disintegration/s, k is the conversion factor $1.602\text{x}10^{-10}$ Gy g MeV^{-1}, n is the number of quanta of energy E emitted per disintegration, and $\Phi(r)$ is the point-isotropic specific absorbed fraction, *i.e.*, the fraction of the emitted energy per gram at a distance r from the point-isotropic source. Perhaps reasonable starting points for our discussions here is the work by Berger (1968) for photons from point-isotropic sources and by Loevinger and Berman (1968) for beta particles from point-isotropic sources.

5.1. Photons

For the more general case of a radionuclide that emits a number of photon energies, the absorbed-dose rate is obtained by summing over the emissions:

$$\dot{D}(r) = A k \sum_i n_i E_i \Phi_i(r). \tag{2}$$

For each photon energy E_i, the determination of photon point kernels requires knowledge of the exponential attenuation (*i.e.*, the total attenuation coefficient, μ) of the photon out to the distance r of interest, the mass energy-absorption coefficient, $\frac{\mu_{en}}{\rho}$, to convert the photon fluence to absorbed dose, and the energy-absorption buildup factor, B_{en}, that accounts for the increase in absorbed dose due to scattered photons. Thus for photons the point kernel is

$$\Phi(r) = \frac{\mu_{en}}{\rho} \frac{B_{en}(\mu r)}{4\pi r^2} e^{-\mu r}, \tag{3}$$

[10] An authoritative definition of the point kernel seems a bit elusive. I prefer the form indicated later in eq. (12), but the concept is, in any case, quite clear. Recently the point kernel seems to be called the dose point kernel (DPK) in medical physics applications.

where the subscript i on the energy-dependent parameters is now understood. Using their then current data for the attenuation and energy-absorption coefficients and moments-method results for the buildup factor, Berger (1968) tabulated point kernels for mono-energetic photons, in water, with energies from 15 keV to 2 MeV. Chen and Nath (2001) recently used Berger's data to estimate absorbed-dose rates from ^{125}I, ^{103}Pd and ^{192}Ir interstitial sources, treating them as simple point sources and obtaining results that are in rather good agreement with detailed Monte Carlo treatments. The main non-trivial quantity required to implement a photon point-kernel calculation is the energy-absorption buildup factor. A fairly recent review of buildup-factor calculations is given in Harima (1993). An example of a general geometry point-kernel code, QAD, that uses such buildup factors is discussed by Tsoulfanidis and Phillips (1991).

The work of Meisberger, Keller, and Shalek (1968) falls into the photon point-kernel category. They fit the average of results from measurement and Berger's (1968) calculations with a third-order polynomial for point sources of ^{60}Co, ^{137}Cs, ^{198}Au and ^{192}Ir. Monte Carlo calculations of point kernels for photon emitters in a water medium using the EGS4 code were done by Furhang, Sgouros, and Chui (1996), who give their results for 14 radionuclides of interest in nuclear medicine, and by Luston and Jozsef (1999), who give results for mono-energetic photons with energies from 10 keV to 20 MeV. In both these calculations, the effects of secondary electron (and positron) transport is included in the results. For a non-point (extended) source, the dose-rate distribution can be obtained by straight-forward superposition, but this assumes that the source and phantom materials are the same. This is not the case for many brachytherapy sources. Approaches based on the use of the Sievert integral have been used, but in its pure form such a method ignores the contribution from scattered photons. To correct for this a number of more elaborate methods have been developed (see, *e.g.*, the recent report of Karaiskos *et al.*, 2000, and references therein). Janicki, Duggan, Rahdert (2001) in their calculations for a photon-emitting stent use a product of the Sievert integral and Berger's (1968) point kernels for water in what they call a Sievert-DPK model[10].

We have developed a photon point-kernel calculation as part of work concerned with hot-particle dosimetry (NCRP, 1999). Buildup factors for a point-isotropic source in water were obtained from ETRAN calculations for energies from 2 MeV down to about 5 keV and for radial distances out to eight mean-free paths. Buildup factors for greater distances were obtained by extrapolation, plotting $B_{en}^{-1}(E,\mu r)$ vs. μr^{-1}, which goes to zero as μr goes to infinity, as indicated in figure 14. In addition, a transition function[11] was extracted from the Monte Carlo calculations that accounts for the net migration away from the point source of energy transferred to secondary electrons and eventually deposited in the water medium. The transition function is shown in figure 15 as a universal curve when plotted against the radial distance from the point source, scaled to an "effective" range, which is the weighted average of the csda[12] ranges of secondary electrons produced in the interaction. The effective range parameter is listed in table 4 as a function of photon energy.

[11] This transition occurs over a distance associated with the secondary-electron range, beyond which electron equilibrium is assumed.

[12] The acronym for the "continuous-slowing-down approximation."

Assuming the source volume V is uniformly emitting, the absorbed-dose rate at position $\vec{r}$ in the medium, from a photon of energy E, is then obtained by a three-dimensional integral:

$$\dot{D}(\vec{r}) = \frac{AknE}{4\pi V}\left(\frac{\mu_{en}}{\rho}\right)_{med} \int_V T(E, s\rho_{wat}) B_{en}(E,u) \frac{e^{-u}}{\left|\vec{r} - \vec{r}'\right|^2} \mathrm{d}V , \qquad (4)$$

where T is the transition function, assuming $s\rho_{wat} = \sum_j t_j \rho_j$ is the accumulated mass pathlength from emission point $\vec{r}'$ to dose point $\vec{r}$ (made up of a series of pathlengths t_j through materials of density ρ_j), and $u = \sum_j \left(\frac{\mu}{\rho}\right)_j t_j \rho_j$ is the similarly defined accumulated number of photon mean-free paths. The total absorbed dose is a summation of results from eq. (4) for all photons of E and emission probability n in the decay of the radioisotope. The numerical integration over the source volume is performed using an adaptive quadrature routine of Genz and Malik (1980). Note that although the correct attenuation coefficients are used for the materials involved, the dose buildup (as is the transition function) is based only on water results. As Berger (1968) showed, water buildup factors should be a good approximation to other low-Z tissues and phantom materials. This would seem also to be not too bad an approximation when the metal components contribute only a small fraction of a mean-free path to an emerging photon, and so might be more applicable to medium-energy emitters such as ^{192}Ir than to low-energy emitters such as ^{125}I.

The results of this point-kernel calculation for the Best Industries ^{192}Ir seed can be compared with the Monte Carlo results of Thomason *et al.* (1991) and Thomason (1992) who used EGS4 to calculate the dose distribution in water. The seed is modeled as a right circular cylinder of 70% Pt/30% Ir, 3 mm in length and 0.1 mm in diameter, encapsulated by a 0.2 mm thick cylindrical steel sheath of the same length. For our point-kernel calculations, the emission spectrum given in table 5 was used. The relative radial dose-rate distributions are compared in table 6, cast in terms of the TG43 radial dose function defined by Nath *et al.* (1995). The point-kernel results agree to within 2% of the Monte Carlo results of Thomason *et al.*, within their stated statistical uncertainty of ~2.5%. This would not seem to be a particularly rigorous test as the Monte Carlo results are stated to agree within their uncertainty with the results using Berger's (1968) point kernels for an unclad point source. The listed TG43 values for the radial dose function seem to fall off a bit too rapidly, due perhaps to reliance on measured data in phantoms that were too small to ensure full scatter buildup (R. Nath, private communication).

5.2. Beta Particles

The absorbed-dose rate from beta particles can be written (Loevinger and Berman, 1968), in analogy with eq. (1), as

$$\dot{D}(r) = Akn_\beta E_{av} \Phi_\beta(r) , \qquad (5)$$

where n_β is the number of beta particles emitted per disintegration, E_{av} is the mean energy of the beta spectrum, and

$$\Phi_\beta(r) = \int_0^{E_{max}} (E_o/E_{av}) S_\beta(E_o) \Phi(r,E_o) \, dE_o, \quad (6)$$

is the beta point kernel. In eq. (6), $S_\beta(E_o)$ is the beta source spectrum with end-point energy E_{max}, and $\Phi(r,E_o)$ is the point kernel for the mono-energetic source of energy E_o. If all of the emitted energy is assumed to be absorbed somewhere in the medium, one has the normalization condition

$$4\pi\rho \int_0^\infty r^2 \Phi_\beta(r) \, dr = 1. \quad (7)$$

For complex beta spectra, eq. (5) is generalized to a summation as in eq. (2). However, the summation can be performed on the constituent beta point kernels and the parameters n_β and E_{av} reinterpreted, so that one can then evaluate eq. (5) as written.

Based on fits of available measured data for beta emitters, Loevinger (1954, 1956) gave a set of formulae for the absorbed dose as a function of distance in a homogeneous medium from a point source. His characterization involves simple exponential functions and basically two parameters that depend only on the end-point energy and the average energy of the beta spectrum. The density of the (assumed low-Z) medium enters to preserve units and provide for proper scaling. The distribution is normalized so that its integral over all space returns the mean energy of the beta particles emitted per disintegration. Although a number of more accurate results are now available, Loevinger's empirical formula is still sometimes used because it can be analytically integrated in applications to a number of pertinent geometries.

Spencer (1959) used his moments-method calculation (Spencer, 1955) to tabulate dose distributions[13] for point-isotropic sources of mono-energetic electrons, with kinetic energies from 25 keV to 10 MeV in carbon, aluminum, copper, tin, lead, air and polystyrene, that could be interpolated to other source energies and absorbing media. Cross (1967a, 1967b), interpolating/integrating over Spencer's results, found good agreement between calculated and measured point-source dose distributions and published point kernels for 40 radionuclides in air and water, later extending this to 95 radionuclides (Cross *et al.*, 1982). Also using Spencer's results, Berger (1971) prepared tables for mono-energetic sources with energies from 25 keV to 4 MeV, and for 75 radionuclides, in an effective scaled form. Although he obtained his point kernels using different numerical procedures, Berger found very few cases of appreciable differences with those of Cross. The VARSKIN code (Durham, Reece, and Merwin, 1991) is based on the use of Berger's (1971) point kernels. Based on fits to Berger's point kernels, Vynckier and Wambersie (1982, 1986) proposed a modification to Loevinger's empirical formulae involving an additional term and a new fitting parameter that could be used to bring the curves for specific beta spectra into better agreement with Cross' and Berger's results.

Point kernels more recently have been calculated with Monte Carlo codes. Using the ETRAN code, Berger (1973) obtained point kernels for mono-energetic electrons with energies up to 10

[13] This calculation was done in the continuous-slowing-down approximation, and neglects the production and transport of secondary electrons and bremsstrahlung.

MeV in an infinite water medium. These results are somewhat in error due to a defective energy-loss straggling algorithm in ETRAN. This was corrected (Seltzer, 1988), and new point kernels were calculated by Seltzer (1991) for electron energies from 20 keV to 20 MeV. Cross *et al.* (1992) obtained mono-energetic point kernels for electrons with energies from 20 keV to 4 MeV from calculations with the ACCEPT code, and integrated them for 147 beta emitters. Using the EGS4 code, Simpkin and Mackie (1990) calculated point kernels for 8 beta emitters. The various point-kernel results are compared in figure 16 for ^{90}Y. The more recent Monte Carlo results generally show smaller absorbed doses close to the source and larger absorbed doses at greater distances when compared to the results of Cross (1967a, 1967b) and of Berger (1971) done in the csda. Loevinger's empirical results are also included, and can be seen to be rather approximate.

It has long been noticed that various transport results, particularly depth-dose curves, are somewhat similar when depth is cast in terms of fractions of the csda range. The csda range, an integral over the reciprocal of the stopping power, tends to remove the dependence on the initial electron energy. The similarity is strong when the atomic number Z of the media are not too different. For the broad beta spectra, Cross (1968; see also Cross *et al.*,1992; ICRU, 1997) developed a more phenomenological scaling rule from a systematic analysis of results for beta-particle point kernels. In this approximate scaling, the absorbed dose[14] $D(r)$ at a distance r (in cm) in a medium is related to the absorbed dose in water, $D_w(\eta r)$, at distance ηr by

$$D(r) = \eta^3 \frac{\rho^2}{\rho_w^2} D_w\left(\eta \frac{\rho}{\rho_w} r\right), \tag{8}$$

where η is the scaling factor of the medium relative to water, and ρ and ρ_w are the densities of the medium and water, respectively. The factor $\eta^3 \frac{\rho^2}{\rho_w^2}$ is included to satisfy the normalization requirement that the total energy emitted must be absorbed in either medium. Note that for a medium that differs only in density, η is unity, and the scaling is exact, reducing to the density scaling underlying the schema of Loevinger and Berman (1968). Cross uses the ratio of the csda mass range in water[15] to that in the medium for 500 keV electrons to serve as a measure of the mass-stopping-power ratio. He then surmised that the remainder of the Z dependence is a reflection of differences in elastic scattering, and defined an effective atomic number $\bar{Z}$ as

$$\bar{Z} = \frac{\sum_i w_i Z_i^2 / A_i}{\sum_i w_i Z_i / A_i}, \tag{9}$$

where w_i is the fraction by weight of the atomic number Z_i and mass A_i, and the summation extends over all elements in the medium. The fitted formula for the scaling factor (Cross *et al.*,

[14] The same relation holds for the corresponding absorbed fractions or point kernels.
[15] Cross (1968) originally cast the relative scaling factor in terms of air as the reference medium.

1992), obtained from measured and calculated point kernels for media with effective atomic numbers from 4 to 18[16], is given by[17]

$$\eta = \left(0.777 + 0.03756\overline{Z} - 0.00066\overline{Z}^2\right)\left(\frac{1}{\rho}r_o\right)_{\text{water}} \Big/ \left(\frac{1}{\rho}r_o\right), \tag{10}$$

where $\left(\frac{1}{\rho}r_o\right)$ is the csda (mass) range evaluated at 500 keV. Cross estimates the accuracy of this scaling function to be 1.5%. Berger (1971), using only his calculated point kernels for effective atomic numbers from about 4 to about 9, developed a somewhat different formula for the scaling factor given by

$$\eta = \left[1.0 + 0.02252\left(\overline{Z} - 6.60\right)\right]\left(\frac{1}{\rho}S_{\text{col}}\right) \Big/ \left(\frac{1}{\rho}S_{\text{col}}\right)_{\text{water}}, \tag{11}$$

where $\left(\frac{1}{\rho}S_{\text{col}}\right)$ is the mass collision stopping power evaluated at 200 keV and $\overline{Z}$ is as defined by Cross. Berger's estimated accuracy of his scaling function is also about 1.5%.

In their theoretical dosimetry study for coated stents, Prestwich, Kennett, and Kus (1995) used the point kernels from Berger's (1973) Monte Carlo results to calculate the dose-rate distribution in the exterior water region around a cylinder whose sides are coated with ^{32}P. In applications to far simpler geometry, Amols, Reinstein, and Weinberger (1996) calculated the dose-rate distribution around a balloon filled with a solution of ^{90}Y, using the point kernel from Simpkin and Mackie (1990), finding good agreement with measurement. Xu *et al.* (1997) used Loevinger's empirical point kernels in their calculations of the dose-rate distribution for a 27 mm ^{32}P line source. Baltas *et al.* (2001) compare their Monte Carlo results with those of their Loevinger point-kernel calculations for the beta component of ^{192}Ir.

Janicki *et al.* (1997) extended the point-kernel calculations of Prestwich *et al.* (1995) for ^{32}P-coated cylindrical segments to model the dose-rate distribution from a Palmaz-Schatz stent. Janicki *et al.* (1999) revisited their calculations for a realistic ^{32}P-coated stent, but applying the Cross scaling method to individual path segments through heterogeneous media in their point-kernel integrations. A similar segment-scaling model was employed by Fox and Henson (2000) in their study of stents coated with ^{188}Re and ^{32}P, using Cross' scaling factors with the point kernels of Simpkin and Mackie (1990). Reynaert and Häfeli (2001) did a theoretical study of the dose-rate distribution around ^{188}Re-, ^{32}P- and ^{198}Au-coated stents by calculating point kernels for the beta spectra using both the EGS4 and the MCNP4B Monte Carlo codes from which they

[16] Cross (1968) finds approximate scaling even for atomic numbers up to 82, but a fitted formula would be different from that given in eq. (10) and presumably would have a poorer stated accuracy.

[17] Cross writes eq. (10) in terms of a stopping-power ratio, as is used in eq. (11), but evaluates the expression as written here. There would not seem to be a choice in how this ratio is evaluated, either in eq. (10) or eq. (11), as this quantity has been factored out of measured or calculated point kernels to deduce the remaining function of $\overline{Z}$ in the prescriptions for the scaling parameter.

found good agreement. In order to incorporate self-absorption effects in the strut material, they calculated also the kernels for point sources at centers of steel spheres with diameters from 10 μm to 1 mm. Their final results integrated over the stent geometry are compared with results using the segment-scaling method of Janicki *et al.* (1999) but with an independent evaluation of the stopping-power ratio used in Cross' scaling factor. They conclude that the use of scaling in these heterogeneous media overestimates the self-absorption effects of the stent components. This issue is further debated in Janicki (2002) and in Reynaert and Häfeli (2002). The use of Cross' scaling is further discussed by Schaart (2002) in application to the dosimetry of a $^{188}W/^{188}Re$ beta line source.

5.3 Some Unpublished NIST Beta Point-Kernel Calculations

A companion code[18] to that described for photon point-kernel calculations handles beta emitters. The calculation is based on the mono-energetic point kernels for water of Seltzer (1991). It is advantageous to use scaled point kernels defined as

$$\begin{aligned} F(r,E_o) &= 4\pi\rho r^2 \Phi(r,E_o), \\ F_\beta(r) &= 4\pi\rho r^2 \Phi_\beta(r), \end{aligned} \tag{12}$$

where ρ is the density of water, included to ensure dimensional consistency. The scaled[19] mono-energetic point kernels are illustrated figure 17. Point kernels for radionuclides are obtained by integration (see eq. (6)) over spectra generated with the LOGFT program (Grove and Martin, 1971) using input from the Evaluated Nuclear Structure Data File from the Brookhaven National Laboratory. The program and data were current in the mid-1980s, but the spectra are expected to still be reliable and are in good agreement with those listed in ICRU (1997). Spectra and resulting point kernels are shown in figure 18 for $^{90}Sr/^{90}Y$, ^{32}P, and ^{133}Xe. Summary data on the emitters are listed in table 7.

For the assumed geometry, the beta point kernels are integrated over the emitting volume (assumed uniform) according to

$$\dot{D}(\vec{r}) = \frac{A k n_\beta E_{av}}{4\pi\rho V} \int_V \frac{F_\beta(s)}{\left|\vec{r} - \vec{r}'\right|^2} \mathrm{d}V , \tag{13}$$

where $s\rho = \sum_j t_j \rho_j$ as defined below eq. (4). Provisions had been included for the use of the segment scaling in inhomogeneous media as more recently outlined by Janicki *et al.* (1999). However, reluctance to use it is based on the sense that when it makes a significant difference it is apt to be inaccurate and when it makes a small difference it can be ignored. A comparison of point-kernel and CYLTRAN Monte Carlo results for the radial dose-rate distribution in an A-150

[18] These codes were called NISTKIN in NCRP (1999) to invoke the similarity in approach and application to VARSKIN.

[19] The scaling used in figure 17 involves a change of variable to $r/r_o(E_o)$, with a multiplicative factor of r_o rendering the plotted function dimensionless.

plastic phantom for the Novoste $^{90}Sr/^{90}Y$ seed is shown in figure 19. In this case, homogeneous-media scaling from water to A-150 plastic was included. The graph includes the results of radiochromic film measurements by Soares (private communication). Figure 20 gives a similar comparison for the Guidant 27 mm ^{32}P source in an A-150 measurement medium. Point-kernel results for a Radiance 3.2 mm diameter ^{32}P-walled, water-filled balloon in water are compared in figure 21 with the radiochromic film measurements of Soares (private communication). In this case the point-kernel results should also closely represent Monte Carlo results as the materials involved are water or nearly water-equivalent.

Finally, point-kernel results in a water phantom are given for a balloon filled with ^{133}Xe-laced gas as proposed by Apple and Waksman (1999). Again, because the materials involved are nearly water-equivalent, only density scaling has been used. One of the resultant radial dose-rate distributions is shown in figure 22, and tables 8a-c give dose-rate results at 0.25 mm from the balloon outer surface in the bisecting plane for a variety of condition.

Summary

Rather accurate Monte Carlo codes are available for the theoretical dosimetry of IVBT sources. Results for the major codes tend to agree with each other to within 3% to 10% for the more difficult case of beta emitters over the range of depths of interest in IVBT; agreement with measurements is usually fairly good, but differences can reach to as much as 10% to 30%. However, some care should be taken in understanding the algorithms and cross sections used by the code(s) and in choosing the proper parameters for a particular calculation. The dosimetry measurements at NIST currently carry a 15% uncertainty (at the 95% confidence level), so it is difficult to make the determination that the Monte Carlo calculations have significant inherent defects. The source term used in calculations is usually based on the assumption of simple uniformity, so at least small differences from the real world can be expected. Point-kernel calculations can be a valuable adjunct to Monte Carlo, as they are typically 2 to 3 orders of magnitude faster. For a number of IVBT problems involving inhomogeneous media, differences with Monte Carlo results is perhaps as large as 10% to 15% at distances of usual interest, and can be greater at larger distances[20]. Even so, such a level of agreement might be acceptable for a number of problems.

6. Acknowledgements

Much of this material accumulated over the last 7 years, and a number of my colleagues have contributed directly and indirectly. In particular, Chris Soares of NIST has helped define many of the issues in this area and provided measurement results. Firas Mourtada at NIST and then at Guidant Corporation has been generous with information, helping in early comparisons of Monte Carlo calculations and more recently in discussions about possible modeling artifacts. Paul Bergstrom of NIST was of invaluable help in setting up and running the comparison calculations with the MCNP4C, EGS4, EGSnrc, and PENELOPE codes for this manuscript, on very short notice and with a very short deadline. And my thanks to John DeMarco and Dennis Schaart who provided pre-print material that helped in my better understanding of the MCNP code.

[20] It can no doubt be argued that improved point-kernel models are possible. It would seem, however, that point-kernel approaches could not reproduce dose perturbations close to the interface separating two materials of significantly different atomic numbers, a situation not uncommon in these applications.

REFERENCES

Amols, H.I, Reinstein, L.E. and Weinberger, J. (1996). "Dosimetry of a radioactive coronary balloon dilitation catheter for treatment of neointimal hyperplasia," Med. Phys. 23:1783-1788.

Andreo, P. (1991). "Monte Carlo techniques in medical radiation physics," Phy. Med. Biol. 36:861-920.

Apple, M. and Waksman, R. (1999). "Xenon 133 Gas-Filled Balloon," Vascular Brachytherapy (Ed., Waksman) Armonk, NY:Futura Publishing Co., pp. 569-578.

Ballester, F., Hernández, C., Pérez-Calatayud, J. and Lliso, F. (1997). "Monte Carlo calculation of dose rate distributions around ^{192}Ir wires," Med. Phys. 24:1221-1228.

Ballester, F., Puchades, V., Lluch, J.L., Serrano-Andrés, M.A., Limami, Y., Pérez-Calatayud, J. and Casal, E. (2001). "Technical note: Monte-Carlo dosimetry of the HDR 12i and Plus ^{192}Ir sources," Med. Phys. 28:2586-2591.

Baltas, D., Karaiskos, P., Papagiannis, P., Sakelliou, L., Loeffler, E. and Zamboglu, N. (2001). "Beta versus gamma dosimetry close to Ir-192 brachytherapy sources," Med. Phys. 28:1875-1882.

Berger, M.J. (1963). "Monte Carlo calculations of the penetration and diffusion of fast charged particles," *Methods in Computations Physics*, Vol 1. (Alder, B., Fernbach, S. and Rotenberg, M., Eds.), New York: Academic Press, pp. 135-215.

Berger, M.J. (1968). "Energy deposition in water by photons from point isotropic sources," MIRD Pamphlet No. 2, J. Nucl. Med. Suppl. 1:15-25.

Berger, M.J. (1971). "Distribution of absorbed dose around point sources of electrons and beta particles in water and other media," MIRD Pamphlet No. 7, J. Nucl. Med. Suppl. 5, 12:5-23.

Berger, M.J. (1973). *Improved Point Kernels for Electron and Beta-Ray Dosimetry*, Report NBSIR 73-107, National Bureau of Standards, Gaithersburg, MD.

Berger, M.J. and Hubbell, J.H. (1987). *XCOM: Photon Cross Sections on a Personal Computer*, Report NBSIR 87-3597, National Bureau of Standards, Gaithersburg, MD.

Berger, M.J. and Seltzer, S.M. (1964). *Tables of Energy Losses and Ranges of Electrons and Positrons*, Publication SP-3012 (1964), National Aeronautics and Space Administration, Greenbelt, MD; and *Studies in Penetration of Charged Particles in Matter*, Report 1133, National Academy of Science – National Research Council, Washington, DC, p. 205.

Berger, M.J. and Seltzer, S.M. (1966). *Additional Stopping Power and Range Tables for Protons, Mesons and Electrons*, Publication SP-3036, National Aeronautics and Space Administration, Greenbelt, MD.

Berger, M.J. and Seltzer, S.M. (1968). *Electron and Photon Transport Programs, I. Introduction and Notes on Program DATAPAC 4*, NBS Report 9836, and *Electron and Photon Transport Programs, II. Notes on Program ETRAN 15*, NBS Report 9837, National Bureau of Standards, Gaithersburg, MD.

Berger, M.J. and Seltzer, S.M. (1970). "Bremsstrahlung and Photoneutrons from Thick Tungsten and Tantalum Targets," Phys. Rev. C 2:621-631.

Berger, M.J. and Seltzer, S.M. (1982). *Stopping Powers and Ranges of Electrons and Positrons*, Report NBSIR 82-2550-A, National Bureau of Standards, Gaithersburg, MD.

Berger, M.J. and Seltzer, S.M. (2000). *Database of Cross Sections for the Elastic Scattering of Electrons and Positrons by Atoms*, Report NISTIR 6573, National Institute of Standards and Technology, Gaithersburg, MD.

Bhabha, H.J. (1936). "The scattering of positrons by electrons with exchange ON Dirac's theory of the positron," Proc. Roy. Soc. A154:195-206 .

Bielajew, A.F. (2001) "Some Random Thoughts on Monte Carlo Electron and Photon Transport," Advanced Monte Carlo for Radiation Physics, Particle Transport Simulation and Applications, Proceedings of the Monte Carlo 2000 Conference, Lisbon, 23-26 October 2000, (Eds. A. Kling, F. Barão, M. Nakagawa, L. Távora and P. Vaz) Berlin:Springer, pp. 1-6.

Bielajew, A.F. and Rogers, D.W.O. (1986). "Interface artifacts in Monte Carlo calculations," Phys. Med. Biol. 31:301-302.

Bielajew, A.F. and Rogers, D.W.O. (1987). "PRESTA: the parameter reduced selectron-step algorithm for electron Monte Carlo transport," Nucl. Instr. Meth. B18:165-181.

Bielajew, A.F. and Rogers, D.W.O. (1988). "Electron Step-Size Artifacts and PRESTA" *Monte Carlo Transport of Electrons and Photons* (Eds. T.M. Jenkins, W.R. Nelson and A. Rindi), NY:Plenum, pp. 115-137.

Bielajew, A.F., Mohan, R. and Chui, C.S., (1989). *Improved bremsstrahlung photon angular sampling in the EGS4 code system*, Report PIRS-0203, National Research Council of Canada, Ottowa, Canada.

Biggs, F., Mendelsohn, L.B. and Mann, J.B. (1975). "Hartree-Fock Compton profiles for the elements," Atomic Data & Nucl. Data Tables 16:201-309.

Blunck, O. and Leisegang, S. (1950). "Zum Energieverlust schneller Elektronen in dünnen Schichten," Z. Physik. 128:500-505.

Bohm, T.D., Mourtada, F.A. and Das, R.K. (2001). "Dose rate table for a ^{32}P intravascular brachytherapy source from Monte Carlo calculations," Med. Phys. 28:1770-1775.

Briesmeister, J.F. (1993). *MCNP – A General Monte Carlo N-Particle Transport Code, Version 4A*, Report LA-12625-M, Version 4A, Los Alamos National Laboratory, Los Alamos, NM.

Briesmeister, J.F. (1997). *MCNP – A General Monte Carlo N-Particle Transport Code, Version 4B*, Report LA-12625-M, Version 4B, Los Alamos National Laboratory, Los Alamos, NM.

Briesmeister, J.F. (2000). *MCNP – A General Monte Carlo N-Particle Transport Code, Version 4C*, Report LA-13709-M, Los Alamos National Laboratory, Los Alamos, NM.

Brun, R. Bruyant, F., Maire, M., McPherson, A.C. and Zanarini, P. (1986). *GEANT3*, Report DD/EE/84-1, CERN, Geneva.

Chen, Z. and Nath, R. (2001). "Dose rate constant and energy spectrum of interstitial brachytherapy sources," Med. Phys. 28:86-96.

Cho, S.H., Muller-Runkel, R. and Hanson, W.F. (1999). "Determination of the tissue attenuation factor along two major axies of a high dose rate (HDR) ^{192}Ir source," Med. Phys. 26:1492-1497.

Chu, S.Y.K., Ekström, L.P. and Firestone, R.B. (1999). Lund/LBNL Nuclear Data Search, Version 2.0, Feb. 1999, providing the WWW Table of Radioactive Isotopes, maintained by the Lawrence Berkeley Laboratory, Berkeley, USA, and the Department of Physics, Lund University, Sweden; accessed Feb. 2001.

Clarijs, M.C., Bos, A.J.J., van Eijk, C.W.E. and Schaart, D.R. (2000). "Modelling of a ^{188}W/^{188}Re beta line source for coronary brachytherapy by means of EGS4 Monte Carlo simulations," Phys. Med. Biol. 45:1319-1334.

Colbert, H.M. (1974). *SANDYL: A Computer Code for Calculating Combined Photon-Electron Transport in Complex Systems*, Report SLL-74-0012, Sandia National Laboratories, Albuquerque, NM.

Cross, W.G. (1967a). "The distribution of absorbed energy from a point beta source," Can. J. Phys. 45:2021-2040.

Cross, W.G. (1967b). *Tables of Beta Dose Distributions*, Report AECL-2793, Atomic Energy of Canada Limited, Chalk River, Ontario.

Cross, W.G., Ing, H., Freedman, N.O. and Mainville, J. (1982). *Tables of Beta-Ray Dose Distributions in Water, Air and Other Media*, Report AECL-7617, Atomic Energy of Canada Limited, Chalk River, Ontario.

Cullen, D.E, Perkins, S.T. and Rathkopf, J.A. (1990). *The 1989 Livermore Evaluated Photon Data Library (EPDL)*, Report UCRL-ID-103424, Lawrence Livermore National Laboratory, Livermore, CA.

Cullen, D.E, Hubbell, J.H. and Kissel, L. (1997). *EPDL The Evaluated Data Library, '97 Version*, Report UCRL-50400, Vol. 6, Rev. 5, Lawrence Livermore National Laboratory, Livermore, CA.

Datta, R.P. and Ray, A.K. (1993). "A spatial characteristic scheme for multigroup discrete ordinates electron-energy deposition in 2 dimensions," Phyisca Status Soidi B 180:85-95.

Datta, R.P., Ray, A.K. and Wienke, B.R. (1992). "A discrete ordinates study of 2-dimensional electron transport," J. App. Phys. D 26:1077-1083.

Datta, R.P., Hira, A.S., Ray A.K. and Wienke, B.R. (1992). "A note on 2-D electron transport using discrete ordinates," Supercomputer 9:15-21.

Daskalov, G.M., Baker, R.S., Little, R.C., Rogers, D.W.O. and Williamson, J.F. (2000a). "Two-Dimensional Discrete Ordinates Photon Transport Calculations for Brachytherapy Dosimetry Applications," Nucl. Sci Eng. 134:121-134.

Daskalov, G.M., Baker, R.S., Rogers, D.W.O. and Williamson, J.F. (2000b). "Dosimetric modeling of the microselectron high-dose rate ^{192}Ir source by the multigroup discrete ordinates method," Med. Phys. 27:2307-2319.

Daskalov, G.M., Löffler, E. and Williamson, J.F. (1998). "Monte Carlo-aided dosimetry of a new high dose-rate brachytherapy source," Med. Phys. 25:2200-2208.

DeMarco, J.J., Boedeker, K. and Wallace, R.E. (2002). "An analysis of MCNP cross-sectios and tally methods for low-energy photon emitter," Phys. Med. Biol. (submitted).

Drumm, C.R. (1997). "Multidimensional electron-photon transport with standard discrete ordinates codes," Nucl. Sci. Engr. 127:1-21.

Duane, S., Bielajew, A.F. and Rogers, D.W.O. (1989). Use of ICRU-37/NBS radiative stopping powers in the EGS4 system, Report PIRS-0173, National Research Council of Canada, Ottowa, Canada.

Durham, J.S., Reece, W.D. and Merwin, S.E. (1991). "Modelling three-dimensional beta sources for skin dose calculations using VARSKIN MOD2," Radiat. Prot. Dosim. 37:89-94.

Fillipone, W.L, Monahan, S.P., Woolf, S. and Garth, J.C. (1990). "Three-dimensional multiregion Sn soultions of the Spencer-Lewis electron equation," Nucl. Sci. Engr. 105:52-55.

Ford, R.L. and Nelson, W.R. (1978). *The EGS code system – Version 3*, Report SLAC-210, Stanford Linear Accelerator Center, Palo Alto, CA.

Fox, R.A. (2002) . "Intravascula brachytherapy of the coronary arteries," Phys. Med. Biol. 47:R1-R30.

Fox, R.A. and Henson, P.W. (2000). "The dosimetry for a coronary artery stent coated with radioactive ^{188}Re and ^{32}P," Phys. Med. Biol. 45:3643-3655.

Furhang, E.E., Sgouros, G. and Chui, C.-S. (1996). "Radionuclide photon dose kernels for internal emitter dosimetry," Med. Phys. 23:759-764.

Genz, A. and Malik, A.A. (1980). "An adaptive algorithm for numerical integration over an n-dimensional rectangular region," J. Comp. Appl. Math 6:295-302.

Goudsmit, S. and Saunderson, J.L. (1940). "Multiple scattering of electron," Phys. Rev. 57:24-29.

Grove, N.B. and Martin, M.J. (1971). "Log-f tables for beta decay," Nucl. Data Tables 10:205-317.

Häfeli, U.O., Roberts, W.K., Meier, D.S., Ciezki, J.P., Pauer, G.J., Lee, E.J. and Weinhous, M.S. (2000). "Dosimetry of a W-188/Re-188 beta line source for endovascular brachytherapty," Med. Phys. 27:668-675.

Haggmark, L.G., MacCallum, C.J. and Riley, M.E. (1974). "New Scattering Cross Sections for Electron Transport," Trans. Amer. Nucl. Soc. 19:471- 472.

Halbleib, J.R. (1980). "ACCEPT: A three-dimensional electron/photon Monte Carlo transport code using combinatorial geometry," Nucl. Sci. Engr. 75:200-201.

Halbleib, J.R. (1988). "Structure and Operation of the ITS Code System," *Monte Carlo Transport of Electrons and Photons* (Eds. T.M. Jenkins, W.R. Nelson and A. Rindi), NY:Plenum, pp. 249-262.

Halbleib, J.A., Kensek, R.P., Mehlhorn, T.A., Valdez, G.D., Seltzer, S.M. and Berger, M.J. (1992a. *ITS Version 3.0: The Integrated TIGER Series of Coupled Electron/Photon Monte Carlo Transport Codes*, Report SAND91-1634, Sandia National Laboratories, Albuquerque, NM.

Halbleib, J.A., Kensek, R.P., Mehlhorn, T.A., Valdez, G.D., Seltzer, S.M. and Berger, M.J. (1992b. "ITS: The Integrated TIGER series of electron/photon Monte Carlo transport codes, IEEE Trans. Nucl. Sci. 73:329-330.

Halbleib, J.A. and Mehlhorn, T.A. (1984). *ITS: The Integrated TIGER Series of Coupled Electron/Photon Monte Carlo Transport Codes*, Report SAND-0573, Sandia National Laboratories, Albuquerque, NM.

Halbleib, J.A. and Mehlhorn, T.A. (1986). "ITS: The integrated TIGER series of coupled electron/photon Monte Carlo transport codes," Nucl. Sci. Engr. 92:338-339.

Halbleib, J.A. and Morel, J.E. (1979). "TIGERP, a one-dimensional multilayer electron/photon Monte Carlo transport code with detailed modeling of atomic shell ionization and relaxation," Nucl. Sci. Engr. 70:213:214.

Halbleib, J.A. and Vandevender, W.H. (1975). "TIGER, a one-dimensional multilayer electron/photon Monte Carlo transport code," Nucl. Sci Engr. 57:94-95.

Halbleib, J.A. and Vandevender, W.H. (1976). "CYLTRAN: A cylindrical-geometry multimaterial electron/photon Monte Carlo transport code," Nucl. Sci. Engr. 61:288-289.

Halbleib, J.A. and Vandevender, W.H. (1977). "Coupled Electron Photon Collisional Transport in Externally Applied Electromagnetic Fields," J. Appl. Phys. 48:2312-2319 .

Harima, Y. (1993). "An historical review and current status of buildup factor calculations and applications," Radiat. Phys. Chem. 41:631-672.

Hendricks, J.S., Frankle, S.C. and Court, J.D. (1994). *ENDF/B-VI Data for MCNP*, Report LA-12891, Los Alamos National Laboratory, Los Alamos, NM.

Hendricks, J.S., Adams, K.J., Booth, T.E., Briesmeister, J.F., Carter, L.L., Cox, L.J., Favorite, J.A., Forster, R.A., McKinney, G.W. and Prael, R.E. (2000). "Present anf future capabilities of MCNP," Appl. Radiat. Isot. 53:857-861.

Hubbell, J.H. (1969). *Photon Cross Scetions, Attenuation Coefficients, and Energy Absorption Coefficients from 10 keV to 100 Gev*, Report NSRDS-NBS 29, National Bureau of Standards, Gaihersburg, MD.

Hubbell, J.H. (1982). "Photon Mass Attenuation and Energy-absorption Coefficients from 1 keV to 20 MeV, Appl. Phys. Isot. 33:1269-1290

Hubbell, J.H., Veigele, W.J., Briggs, E.A., Brown, R.T., Cromer, D.T. and Howerton, R.J. (1975). "Atomic Form Factors, Incoherent Scattering Functions, and Photon Scattering Cross Sections," J. Phys. Chem. Ref. Data 4:471-616.

Hubbell, J.H., Gimm, H.A. and Øverbø, I. (1980). "Pair, Triplet, and Total Cross Sections (and Mass Attenuation Coefficients) for 1 MeV – 100 GeV Photons in Elements Z = 1 to 100," J. Phys. Chem. Ref. Data 9:1023-1147.

International Commission on Radiation Units and Measurements (ICRU). (1984). Report 37, *Stopping Powers and Ranges of Electrons and Positrons*, ICRU, Bethesda, MD.

International Commission on Radiation Units and Measurements (ICRU). (1997). Report 56, *Dosimetry of External Beta Rays for Radiation Protection*, ICRU, Bethesda, MD.

Janicki, C. (2002). "Comment on 'Self-absorption correction for ^{32}P, ^{198}Au and ^{188}Re stents: Dose point kernel calculations versus Monte Carlo'," Med. Phys. 29:260.

Janicki, C., Duggan, D.M., Coffey, C.W., Fischell, D.R. and Fischell, T.A. (1997). "Radiation dose from a phosphorous-32 impregnated wire mesh vascular stent," Med. Phys. 24:437-445.

Janicki, C., Duggan, D.M., Gonzalez, A., Coffey, C.W. and Rahdert, D.A. (1999). "Dose model for a beta-emitting stent in a realistic artery consisting of soft tissue and plaque," Med. Phys. 26:2451-2460.

Janicki, C., Duggan, D.M. and Rahdert, D.A. (2001). "A dose-point-kernel model for a low energy gamma-emitting stent in a heterogeneous medium," Med. Phys. 28:1397-1405.

Karaiskos, P., Angelopoulos, Baras, P., Rozaki-Mavrouli, H., Sandilos, P., Vlachas, L. and Sakelliou, L. (2000). "Dose rate calculations around ^{192}Ir brachytherapy sources using a Sievert integral model," Phys. Med. Biol. 45:383-398.

Kawrakow, I. (2000). "Accurate condensed history Monte Carlo simultion of electron transport. I. EGSnrc, the new EGS4 version," Med. Phys. 27:485-498.

Kawrakow, I. and Bielajew A.F. (1998). "On the representation of electron multiple elastic-scattering distributions for Monte Carlo calculations," Nucl. Instr. Meth B 134:325-336.

Koch, W. and Motz, J.W. (1959). "Bremsstrahlung Cross-Section Formulas and Related Data," Rev. Mod. Phys. 31:920-955.

Landau, L. (1944). "On the Energy Loss of Fast particles by Ionization," J. Phys. (USSR) 8:201-207.

Lewis, H.W. (1950). "Multiple Scattering in an Infinite Medium," Phys. Rev. 78:526-529.

Li, X.A. (2001). "Dosimetric effects of contrast media for catheter-based intravascular brachytherapy," Med. Phys. 28:757-763.

Li, X.A. and Shih, R. (2001). "Dose effects of guide wires for catheter-based intravascular brachytherapy," Intl. J. Radiat. Oncol. Biol. Phys. 51:1103-1110.

Li, A.N., Eigler, N.L., Litvak, F. and Whiting, J.S. (1998). "Characterization of a positron emitting V48 nitinol stent for intracoronary brachytherapy," Med. Phys. 25:20-28.

Li, X.A, Wang, R.Q., Yu, C. and Suntharalingam, M. (2000). "Beta versus gamma for catheter-based intravascular brachytherapy: Dosimetric perspectives in the presence of metallic stents and calcified plaques," Intl. J. Radiat. Oncol. Biol. Phys. 46:1043-1049.

Loevinger, R. (1954). "The dosimetry of beta radiations," Radiology 62:74-82.

Loevinger, R. (1956). "The dopsimetry of beta sources in tissue. The point source function," Radiology 66:55-62.

Loevinger, R. and Berman, M. (1968). "A schema for absorbed-dose calculations for biologically distributed radionuclides," MIRD Pamphlet No. 1, J. Nucl. Med. 9:7-14.

Lorence, L.J. (1992). "CEPXS ONELD version 2.0 – A discrete ordinates code package for general one-dimensional coupled electron-photon transport," IEEE Trans. Nucl. Sci. 39:1031-1034.

Lorence, L.J. and Morel, J.E. (1992). "CEPXS/ONELD: a one-dimensional coupled electron-photon discrete ordinates code package," *Deterministic methods in radiation transport*, Report ORNL/RSIC-54, Oak Ridge National Laboratory, Oak Ridge, TN.

Lorence, L.J., Morel, J.E. and Valdez, G.D. (1989a). *Physics guide to CEPXS: a multi-group coupled electron-photon cross section generating code*, Report SAND 89-1685, Sandia National Laboratories, Albuquerque, NM.

Lorence, L.J., Morel, J.E. and Valdez, G.D. (1989b). *Users guide to CEPXS/ONEDANT: a one-dimensional coupled electron-photon discrete ordinates code package*, Report SAND 89-1661, Sandia National Laboratories, Albuquerque, NM.

Lorence, L.J., Morel, J.E. and Valdez, G.D. (1990). *Results guide to CEPXS/ONEDANT: a one-dimensional coupled electron-photon discrete ordinates code*, Report SAND 89-2211, Sandia National Laboratories, Albuquerque, NM.

Lorence, L.J., Nelson, W.E. and Morel, J.E. (1985). "Coupled electron-photon transport calculations using the method of discrete ordinates," IEEE Trans. Nucl. Sci. 32:4416-4420.

Luxton, G. and Jozseph, G. (1999). "Radial dose distribution, dose to water and dose rate constant for monoenergetic photon point sources from 10 keV to 2 MeV: EGS4 Monte Carlo model calculations," Med. Phys. 26:2531-2538.

Mason, D., Battista, J., Barnett, R. and Porte, A. (1992). "Ytterbium-169: Calculated physical properties of a new radiation source for brachytherapy," Med. Phys. 19:695-703.

MacPherson, M.S. and Battista, J.J. (1995). "Dose distributions and dose rate constants for new yterrbium-169 brachytherapy seeds," Med. Phys. 22:89-96.

Mainegra, E., Capote, R., and López, E. (2000). "Radial dose functions for ^{103}Pd, ^{125}I, ^{169}Yb and ^{192}Ir brachytherapy sources: an EGS4 Monte Carlo study," Phys. Med. Biol. 45:703-717.

Meisberger, L.L., Keller, R.J. and Shalek, R.J. (1968). "The effective attenuation in water of the gamma rays of gold 198, iridium 192, cesium 137, radium 226, and cobalt 60," Radiology 90:953-957.

Molière, G. (1947). "Theorie der Streuung schneller geladener Teilchen I. Einzelstreuung am abgeschirmten Coulomb-Feld," Z. Naturforsch. 2a:133-145.

Molière, G. (1948). "Theorie der Streuung schneller geladener Teilchen II. Mehrfacund and Vielfachstreuung," Z. Naturforsch. 3a:78-79.

Møller, C. (1932). "Zur Theorie des Durchgangs schneller Elektronen durch Materie," Ann. Physik 14:531-585.

Morel, J.E. (1979). "Discrete ordinates electron-transport calculations using standard neutron-transport codes," Trans. Amer. Nucl. Soc. 33:676-677.

Morel, J.E. and Wienke, B.R. (1982). "Advances in discrete-ordinates electron transport," Trans. Amer. Nucl. Soc. 41:475-476.

Mott, N.F. (1929). "The Scattering of Fast Electrons by Atomic Nuclei," Proc. Roy. Soc. (London) A124:425.

Mourtada, F.A., Soares, C.G., Seltzer, S.M. and Lott, S.H. (2000). "Dosimetry characterization of a ^{32}P catheter-based vascular brachytherapy source wire," Med. Phys. 27:1770-1776.

Nagel, H.H. (1965). "Elektron-Photon-Kaskaden in Blei: Monte-Carlo-Rechnungen für eine Primärelektronenergie zwischen 100 und 1000 MeV," Z. Physik 186:319-346.

Nagel, H.H. and Schlier, C. (1963) "Berechnung von Elektron-Photon-Kaskaden in Blei für eine Primärenergie von 200 MeV," Z. Physik 174:464-471.

Nahum, (1988). "An Overview of Photon and Electron Monte Carlo," *Monte Carlo Transport of Electrons and Photons* (Eds. T.M. Jenkins, W.R. Nelson and A. Rindi), NY:Plenum, pp. 3-20.

Nath, R., Anderson, L.L., Luxton, G., Weaver, K.A., Williamson, J.F. and Meigooni, A.S. (1995). "Dosimetry of the interstitial brachytherapy sources: Recommendations of the AAPM Radiation Therapy Committee Task Group No. 43," Med. Phys. 22: 209-234.

Nath, R., Amols, H., Coffey, C., Duggan, D., Jani, S., Li, Z., Schell, M., Soares, C., Whiting, J., Cole, P.E., Crocker, I. And Schwartz, R. (1999). "Intravascular brachytherapy physics: Report of the AAPM Radiation Therapy Committee Task Group No. 60," Med. Phys. 26:119-152.

National Council on Radiation Protection and Measurements (NCRP). (1999). Report 130, *Biological Effects and Exposure Limits for "Hot Particles*," NCRP, Bethesda, MD.

National Nuclear Data Center (2001). Nuclear data from NuDat, a web-based database maintained by the National Nuclear Data Center, Brookhaven National Laboratory, Upton, NY; last database update reported as Feb. 23, 2000; accessed Feb. 2001.

Nelson, W.R., Hirayama, H. and Rogers, D.W.O. (1985). *The EGS4 Code System*, Report SLAC-265, Stanford Linear Accelerator Center, Palo Alto, CA.

Pérez-Calatayud, J., Lliso, F., Carmona, V., Ballerter, F. and Hernández, C. (1999). "Monte Carlo calculation of dose rate distributions around 0.5 and 0.6 mm in diameter ^{192}Ir wires," Med. Phys. 26:395-401.

Perkins, S.T., Cullen, D.E., Chen, M.H., Hubbell, J.H., Rathkopf, J., and Scofield, J. (1991). *Tables and Graphs of Atomic Subshell and Relaxation Data Derived from the LLNL Evaluated Atomic Data Library (EADL), Z=1-100*, Report UCRL-50400, Vol. 30, Lawrence Livermore National Laboratory, Livermore, CA.

Prestwich, W.V., Kennett, T.J. and Kus, F.W. (1995). "The dose distribution produced by a ^{32}P-coated stent," Med. Phys. 22:313-320.

Rashid, H., Bjarngard, B.E., Chin, L.M. and Rice, R.K. (1992). "Dosimetry of 125I sources in a low-density material using scaling," Med. Phys. 20:765-768.

Reynaert, N. and Häfeli, U.O. (2001). "Self-absorption correction for ^{32}P, ^{198}Au and ^{188}Re stents: Dose point kernel calculations versus Monte Carlo," Med. Phys. 28:1883-1897.

Reynaert, N. and Häfeli, U. (2002). "Response to Dr. Janicki's Letter to the Editor," Med. Phys. 29:261.

Reynaert, N., Verhaegen, F., Taeymans, Y., Van Eijkeren, M. and Thierens, H. (1999). "Monte Carlo calculations of dose distributions around ^{32}P and ^{198}Au stents for intravascular brachtherapy," Med. Phys. 26:1484-1491.

Reynaert, N., Van Eijkeren, M., Taeymans, Y. and Thierens, H. (2001). "Dosimetry of ^{192}Ir sources used for endovascular brachytherapy," Phys. Med. Biol. 46:499-516.

Riley, M.E., MacCallum, C. and Biggs, F. (1975). "Theoretical electron-atom elastic scattering cross sections," Atomic Data & Nucl. Data Tables, 15:443-476.

Rogers, D.W.O., Duane, S., Bielajew, A.F. and Nelson, W.R. (1989). *Use of ICRU-37/NBS radiative stopping powers in the EGS4 system*, Report PIRS-0177, National Research Council of Canada, Ottowa, Canada.

Salvat, F., Fernández-Vera, J.M., Acosta, E., and Sempau, J. (2001). *PENELOPE – A Code System for Monte Carlo Simulation of Electron and Photon Transport*, Workshop Proceedings, Issy-les-Moulineaux, France, 5-7 November 2002, OECD Nuclear Energy Agency, Paris.

Schaart, D.R. (2002). "The scaling method applied to beta line sources with a finite diameter," Med. Phys. (submitted).

Schaart, D.R., Jansen, J.T.M., Zoetelief, J. and de Leege, P. (2002a). "A comparison of MCNP4C electron transport with ITS 3.0 and experiment at energies between 100 keV and 20 MeV: Influence of voxel size, substeps and energy indexing algorithm," Phys. Med. Biol. (submitted).

Schaart, D.R., Bos, A.J.J., Winkelman, A.J.M. and Clarijs, M.C. (2002b). "The radial depth-dose distribution of a $^{188}W/^{188}Re$ beta line source measured with ultra-thin TLDs in a PMMA phantom," Phys. Med. Biol. (submitted).

Sehgal, V., Li, Z., Palta, J.R. and Bolch, W.E. (2001). "Dosimetric effect of source centering and residual plaque for β-emitting catheter based intravascualr brachytherapy sources," Med. Phys. 28:2162-2170.

Seltzer, S.M. (1988). "An Overview of ETRAN Monte Carlo Methods for Coupled Electron/Photon Transport Calculations," *Monte Carlo Transport of Electrons and Photons* (Eds. T.M. Jenkins, W.R. Nelson and A. Rindi), NY:Plenum, pp. 153-181.

Seltzer, S.M. (1991). "Electron-Photon Monte Carlo Calculations: The ETRAN Code," Appl. Radiat. Isotop. 42:917-941.

Seltzer, S.M. (1993). "Calculation of Photon Mass Energy-Transfer and Mass Energy-Absorption Coefficients," Rad. Res. 136:147-170.

Seltzer, S.M. and Berger, M.J. (1985). "Bremsstrahlung Spectra from Electron Interactions with Screened Atom Nuclei and Orbital Electrons," Nucl. Instr. Methods B12:95-134.

Seltzer, S.M. and Berger, M.J. (1986). "Bremsstrahlung Energy Spectra from Electrons with Kinetic Energy 1 keV-10 GeV Incident on Screened Nuclei and Orbital Electrons of Neutral Atoms with Z = 1 - 100," Atomic Data & Nucl. Data Tables 35:345-418.

Simpkin, D.J. and Mackie, T.R. (1990). ""EGS4 Monte Carlo determination of the beta dose kernel in water," Med. Phys. 17:179-186.

Soares, C.G., Halpern, G.G. and Wang, C.-K. (1998). "Calibration and characterization of beta-particle sources for intravascular barchytherapy," Med. Phys. 25:339-346.

Spencer, L.V. (1955). "Theory of electron penetration," Phys. Rev. 98:1597-1615.

Spencer, L.V. (1959). *Energy Dissipation by Fast Electrons*, NBS Monograph 1, National Bureau of Standards, Washington, DC.

Stabin, M.G., Konijnenberg, M., Knapp, F.F. and Spencer, R.H. (2000). "Monte Carlo modeling of radiation dose distributions in intravascular radiation therapy," Med. Phys. 27:1086-1092.

Storm, E. and Israel, H.I. (1967). *Photon Cross Sections from 0.001 to 100 MeV for Elements 1 through 100*, Report LA-3753, Los Alamos Scientific Laboratory, Los Alamos, NM.

Storm, E. and Israel, H.I. (1970). "Photon Cross Sections from 1 keV to 100 MeV for Elements $Z = 1$ to $Z = 100$," Nucl. Data Tables 7:565-681.

Thomason, C., Mackie, T.R., Lindstrom, M.J. and Higgins, P.D. (1991). "The dose distribution surrounding ^{192}Ir and ^{137}Cs seed sources," Phys. Med. Biol. 36:475-493.

Thomason, C. (1992). "radial dose distribution from ^{192}Ir seeds at distances far from the source," Med. Phys. 19:199-201.

Todorovic, M., Cremers, F., Albers, and Schmidt, R. (2000). "Simulation of a ^{32}P Sourcewire and a ^{90}Sr/^{90}Y Sourcetrain Using MCNP4b and EGS4," Advanced Monte Carlo for Radiation Physics, Particle Transport Simulation and Applications, Proceedings of the Monte Carlo 2000 Conference, Lisbon, 23-26 October 2000, (Eds. A. Kling, F. Barão, M. Nakagawa, L. Távora and P. Vaz) Berlin:Springer, pp. 521-527.

Tsoulfanidis, N. and Phillips, K. (1991). "Dose rates for several organs in a human from contaminated soil and hot particles using the QAD computer code," Health Phys. 61:653-663.

Vynckier, S. and Wambersie, A. (1982). "Dosimetry of beta sources in radiotherapy: I. The beta point source function," Phys. Med. Biol. 27:1339-1347.

Vynckier, S. and Wambersie, A. (1986). "Dosimetry of beta sources in radiotherapy: Absorbed dose distributions around plane sources," Radiat. Prtot. Dosim. 14:169-173.

Wallace, S., Wong, T. and Fernando, W. (1998). "Monte Carlo dosimetry of the microselectron HDR ^{192}Ir brachytherapy source using MCNP4A," Australian Ohysical and Engineering Sciences in Medicine 21:11-17.

Wang, R., Li, X.A. and Yu, C.X. (2000). "Evaluation of EGS4/PRESTA multiple0scattering algorithms for ^{90}Sr/^{90}Y intravascular brachytherapy dosimetry," Phys. Med. Biol. 45:2343-2352.

Wang, R. and Li, X.A. (2000). "A Monte Carlo calculation of the dosimetric parameters of ^{90}Sr/^{90}Y and ^{192}Ir SS sources for intravascular brachytherapy," Med. Phys. 27: 2528-2535.

Wang, R. and Li, X.A. (2001a). "Monte Carlo dose calculations of beta-emitting sources for intravascular brachytherapy: A compatison between EGS4, EGSnrc, and MCNP," Med. Phys. 28:134-141.

Wang, R. and Li, X.A. (2001b) . "Monte Carlo characterization of a ^{32}P source for intravascular brachytherapy," Med. Phys. 28:1776-1785.

Wang, R. and Sloboda, R.S. (1996). "EGS4 calculations for cylindrically symmetric brachytherapy sources," Med. Phys. 23:1459-1465.

Wang, R. and Sloboda, R.S. (1998a). "Monte Carlo dosimetry of the VariSource high dose rate ^{192}Ir source," Med. Phys. 25:415-423.

Wang, R. and Sloboda, R.S. (1998b). "Influence of source geometry and materials on the tranverse axis dosimetry of ^{192}Ir brachytherapy sources," Phys. Med. Biol. 43:37-48.

Wierzbeicki, J.G., Rivard, M.J., Waid, D.S. and Arterbery, V.E. (1998). "Calculated dosimetric parameters of the IoGold ^{125}I source model 3631-A," Med. Phys. 25:2197-2199.

Williamson, J.F. (1988). "Monte Carlo evaluation of specific dose constants in water for 125I seeds," Med. Phys. 15:686-694.

Williamson, J.F. (1991). "Comparison of measured and calculated dose-rates in water near I-125 and Ir-192 seeds," Med. Phys. 18:776-786.

Xu, Z., Reinstein, L.E., Yang, G., Pai, S., Gluckman, G. and Almond, P.R. (1997). "The investigation of 32P wire for catheter-based endovascular irradiation," Med. Phys. 24:1788-1792.

Ye, S.-J., Li, X.A., Zimmer, J.R., Chu, J.C. and Choi, C.K. (2000). "Dosimetric perturbations of linear array of β-emitter seeds and metallic stent in intravascular brachytherapy," Med. Phys. 27:374-380.

Table 1. Dimensions of cylindrical structures used to simulate the Guidant ^{32}P source, in catheter, in a water medium. The cylindrical structures are centered on the z-axis, at z=0; the dimensions are given only for one half of the problem, with symmetry about the plane perpendicular to the axis at z=0. Compositions of the materials are given in table 2.

z_{min}, cm	z_{max}, cm	r_{min}, cm	r_{max}, cm	Material
0.0	1.0	0.0	0.01015	core
0.0	1.0	0.01015	0.01205	polyimide
0.0	1.0	0.01205	0.01524	air
1.0	1.1	0.0	0.0135	W
1.0	1.1	0.0135	0.01524	air
0.0	1.2	0.01524	0.02285	nitinol
1.2	1.5	0.0	0.02285	nitinol
0.0	1.5	0.02285	0.02985	air
0.0	1.5	0.02985	0.04445	nylon 12
0.0	1.5	0.04445	1.04445	water phantom

Table 2. Composition and density of the materials used in the calculations for the Guidant ^{32}P source.

Material	Density g/cm^3	Composition element/fraction by weight
Core: ethanol glycol, rayon	1.1155	H/0.097432, C/0.387026, O/0.515542
Polyimide	1.096	H/0.026362, C/0.691133, N/0.073270, O/0.209235
Air	0.001205	C/0.000124, N/0.7555267, O/0.231781, Ar/0.012827
Nitinol	6.5	Ti/0.44, Ni/0.56
Nylon 12	1.196	H/0.11749, C/0.73045, N/0.07098, O/0.08108
W	19.3	W/1.0
Water	1.0	H/0.111894, O/0.888106

Table 3. Monte Carlo results for the dose rate in the mid-plane from Guidant ^{32}P sources, given in units of cGy s^{-1} mCi^{-1}. The rates shown in parentheses are scaled from other author's results for a 27 mm source to that for a 20 mm active length by multiplying by 27/20. The PENELOPE results given in italics are from calculations with electron collision stopping powers evaluated for conductors.

	Radial distance of 2 mm			Radial distance of 4 mm		
Source length:	20 mm	27 mm		20 mm	27 mm	
Note:	*a*	*b*	*c*	*a*	*b*	*c*
Code:						
CYLTRAN/ITS3	0.300			0.0276		
MCNP4C	0.314			0.0285		
MCNP4B2	(0.309)	0.229		(0.030)	0.022	
MCNP4B2	(0.313)		0.232	(0.031)		0.023
EGS4	0.296			0.0255		
EGS4	(0.300)	0.222		(0.0261)	0.0193	
EGSnrc	0.296			0.0254		
EGSnrc	(0.300)	0.225		(0.0279)	0.0207	
PENELOPE	0.298			0.0274		
PENELOPE[d]	*0.298*			*0.0290*		

Notes: *a* From this work
b From Wang and Li (2001b)
c From Bohm *et al.* (2001)
d With electron collision stopping powers evaluated for conductors

Table 4. Values of effective range, r_{eff}, the scaled variable in the universal transition function in water for a point-isotropic emitter of photons of energy E.

E, MeV	r_{eff}, g/cm^2	E, MeV	r_{eff}, g/cm^2
2.0	0.853	0.15	0.00530
1.5	0.588	0.10	0.00178
1.25	0.457	0.08	0.00108
1.0	0.328	0.06	0.000748
0.8	0.230	0.05	0.000710
0.6	0.139	0.04	0.000741
0.5	0.0976	0.03	0.000773
0.4	0.0614	0.02	0.000618
0.3	0.0320	0.015	0.000429
0.2	0.0115	0.01	0.000221

Table 5. Assumed ^{192}Ir photon-emission spectrum. The data include lines with energies greater than 10 keV and with emission probabilities greater than 0.01%, and is based on information from the National Nuclear Data Center (2001) and Chu *et al.* (1999). Shaded area indicates x rays.

E (keV)	No./Dis.	E (keV)	No./Dis.	E (keV)	No./Dis.
10.176	0.00042	63.000	0.0207	283.2668	0.00264
10.354	0.00408	65.122	0.0265	295.957	0.2870
10.511	0.00058	66.831	0.0453	308.456	0.2984
10.590	0.00133	71.079	0.00239	316.507	0.8276
10.820	0.000211	71.414	0.00460	329.2	0.00018
10.854	0.00056	71.875	0.000113	374.4852	0.00734
11.071	0.0124	73.363	0.00162	416.47	0.00667
11.235	0.00073	73.590	0.000188	420.53	0.00071
11.242	0.00354	75.368	0.00533	468.07	0.4782
11.562	0.000292	75.749	0.01029	484.58	0.03186
12.096	0.00079	76.233	0.000265	489.05	0.00441
12.422	0.000133	77.831	0.00365	588.58	0.04516
12.500	0.00019	78.073	0.000478	593.4	0.00042
12.942	0.00245	110.093	0.000124	604.41	0.0822
13.271	0.00030	136.343	0.00183	612.46	0.0532
13.273	0.00018	201.3112	0.004725	884.54	0.00292
13.361	0.00025	205.795	0.0332	1061.48	0.000529
61.486	0.0120	280.2	0.00016		

Table 6. Radial dose-rate distributions for the Best Industries ^{192}Ir steel-clad seed, cast in terms of the TG43 radial dose function that is scaled by the line-source geometry factor. The numbers in parentheses were evaluated using the fitted formula given in Nath *et al.* (1995).

r, cm	TG43 Nath *et al.* (1995)	Monte Carlo Thomason *et al.* (1991)	Point-kernel This work
0.05			0.997
0.1	(0.990)		0.996
0.2	(0.991)		0.995
0.3	(0.992)		0.996
0.4	(0.993)		0.996
0.5	0.994		0.997
1	1.00	1.000	1.000
2	1.01	1.011	1.005
3	1.02	1.021	1.009
4	1.01	1.027	1.009
5	0.996	1.028	1.006
6	0.972	1.021	1.000
7	0.942	1.009	0.991
8	0.913	0.996	0.979
9	0.891	0.981	0.964
10		0.961	0.947
11		0.938	0.927
12		0.911	0.905

Table 7. Assumed electron emission data for IVBT calculations. Electron line-emission data pertain to conversion and Auger electrons.

	Continuous Beta Spectra		Electron Line Emission	Photon Line Emission
Nuclide	E_{max} MeV	E_{av} MeV	$\langle E \rangle_{emitted}$ MeV dis^{-1}	$\langle E \rangle_{emitted}$ MeV dis^{-1}
^{32}P	1.7104	0.6949		
^{90}Sr	0.546	0.1958		
^{90}Y	2.2792	0.9326		
$^{90}Sr/^{90}Y$	2.2792	0.5642		
^{133}Xe	0.346	0.1003	0.0373[a]	0.0458[b]

[a] Assumed electron line spectrum (energy/keV, probability/disintegration): 25.4,0.0265; 29.6, 0.0130; 86.6, 0.0364; 45.4, 0.0449; 45.0, 0.5380; 75.3, 0.0701; 80.0, 0.0183; 160.6, 0.00062.

[b] Assumed photon line spectrum (energy/keV, probability/disintegration): 30.9,0.390; 35.1, 0.0911; 81.0, 0.376; 160.6, 0.00062.

Table 8. Dose rates D_β from emitted electrons, and D_γ from emitted photons, in the bisecting plane at a radial distance of 0.25 mm in water from the surface of a cylindrical balloon with no central structures. The 40 mm long balloon, with polyethylene walls, is assumed filled with a mixture of 5% Xe and 95% CO_2 (partial pressures) at 22° C.

a. 3.5 mm OD balloon, 3 atm gas.

Gas		Wall			D_β	D_γ	D_{tot}
P, atm	ρ, g/cm^3	OD, mm	t, mm	ρ, g/cm^3	cGy s^{-1} mCi^{-1}		
3	0.006	3.5	0.050	1.0	0.0697	0.00057	0.0703
3	0.006	3.5	0.050	0.924	0.0721	0.00057	0.0727
3	0.006	3.5	0.045	0.924	0.0751	0.00057	0.0757

b. 3.0 mm OD balloon, 0.040 mm walls.

Gas		Wall			D_β	D_γ	D_{tot}
P, atm	ρ, g/cm^3	OD, mm	t, mm	ρ, g/cm^3	cGy s^{-1} mCi^{-1}		
1	0.002	3.0	0.040	1.0	0.0918	0.00065	0.0925
2	0.004	3.0	0.040	1.0	0.0900	0.00065	0.0907
3	0.006	3.0	0.040	1.0	0.0882	0.00065	0.0827
4	0.008	3.0	0.040	1.0	0.0864	0.00065	0.0871
5	0.010	3.0	0.040	1.0	0.0847	0.00065	0.0854

c. 0.045 mm wall thickness, 3 atm gas.

Gas		Wall			D_β	D_γ	D_{tot}
P, atm	ρ, g/cm^3	OD, mm	t, mm	ρ, g/cm^3	cGy s^{-1} mCi^{-1}		
3	0.006	3.0	0.045	0.924	0.0871	0.00065	0.0878
3	0.006	3.5	0.045	0.924	0.0751	0.00057	0.0757
3	0.006	4.0	0.045	0.924	0.0675	0.00051	0.0680

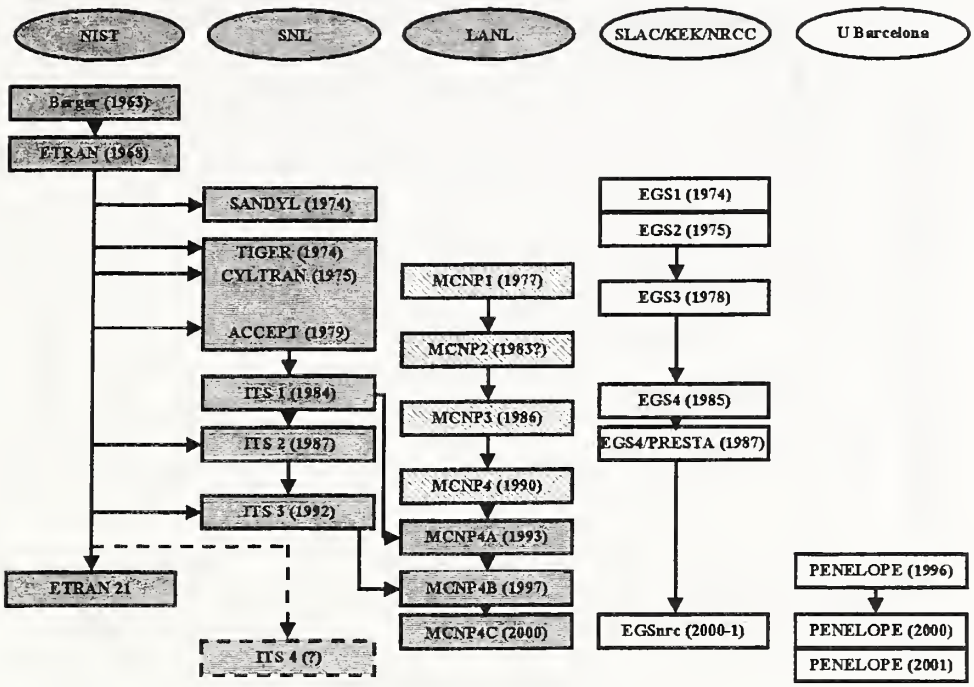

Figure 1. Version history of a number of public-domain, general-purpose coupled electron-photon Monte Carlo transport codes.

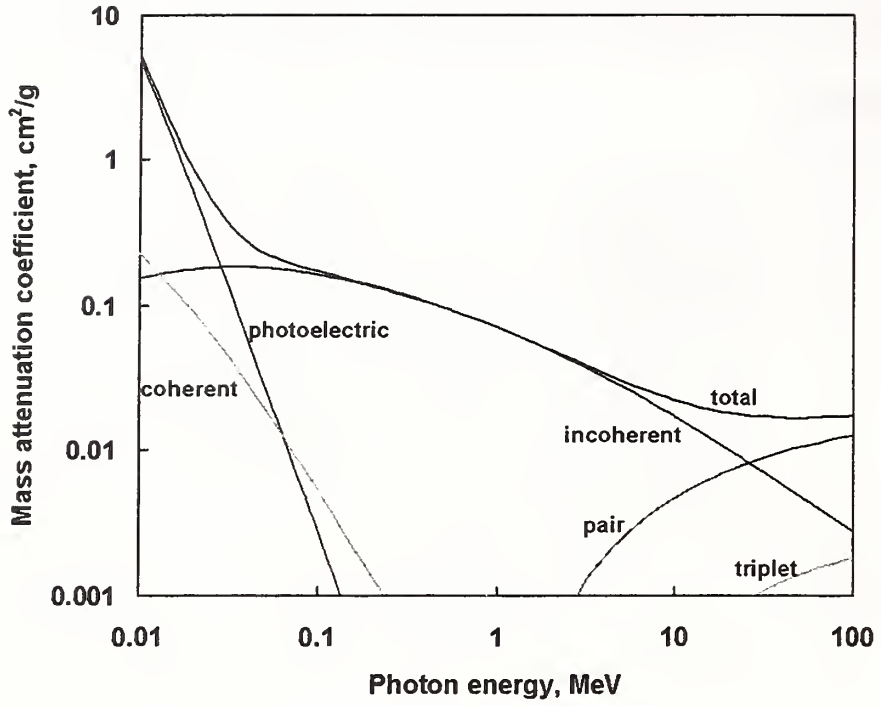

Figure 2. Photon-interaction cross sections in water, given as partial mass attenuation coefficients.

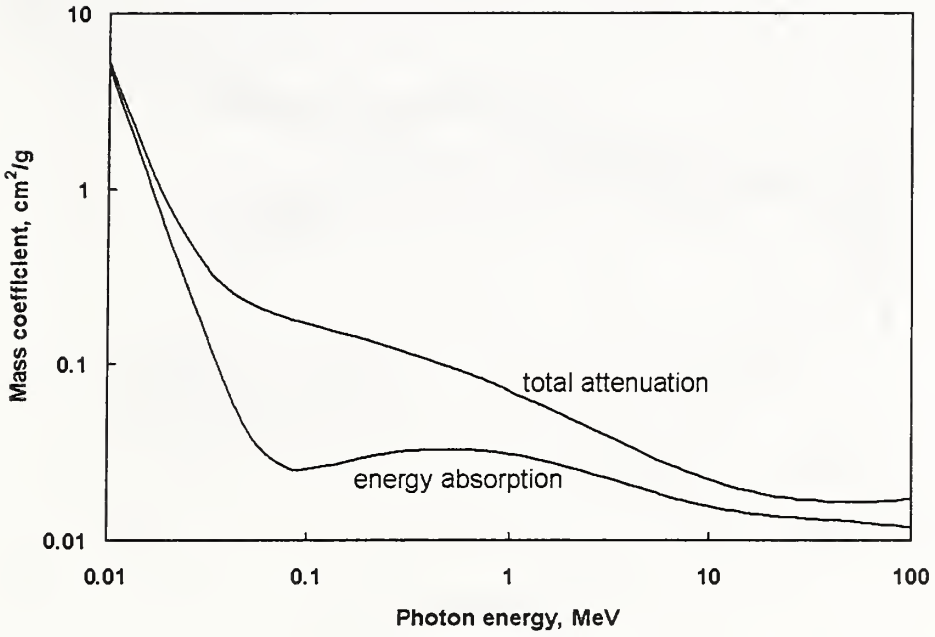

Figure 3. Total mass attenuation and mass energy-absorption coefficients in water.

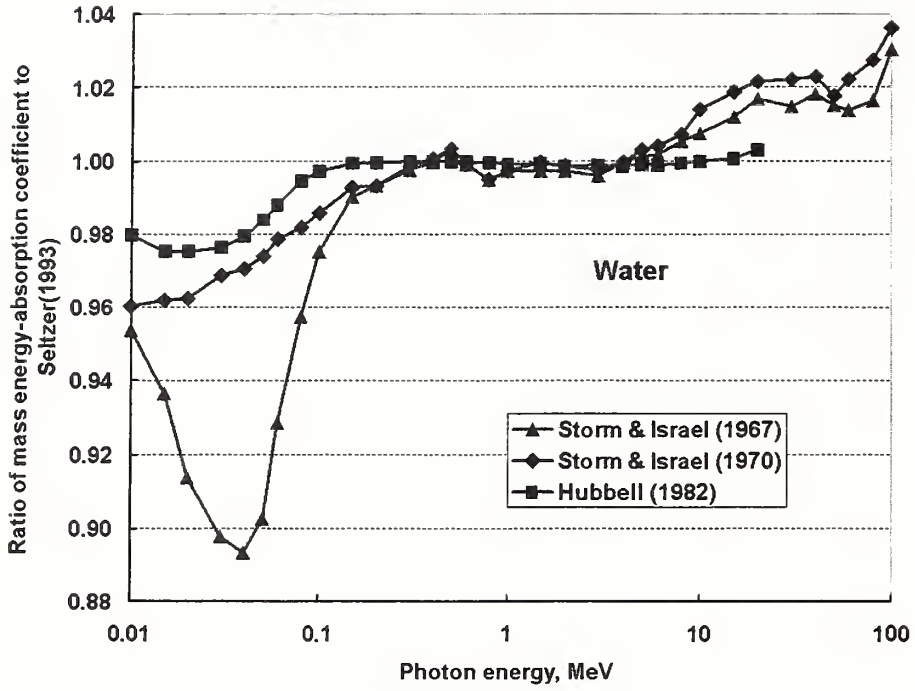

Figure 4. Ratios of the mass energy-absorption coefficients from other authors to those of Seltzer (1993).

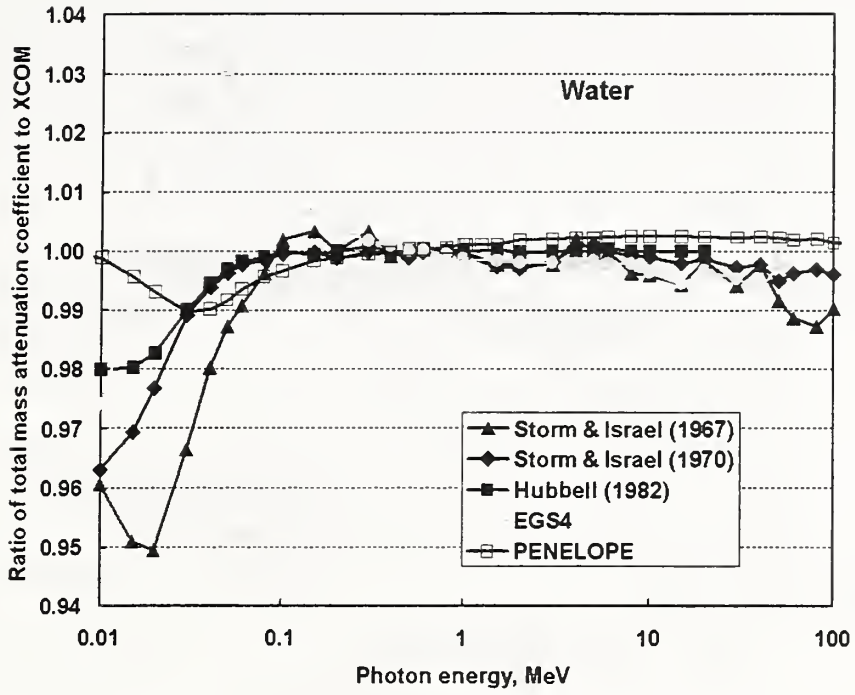

Figure 5. Ratios of total attenuation coefficients for water, from various tabulations, to those from the XCOM database of Berger and Hubbell (1987).

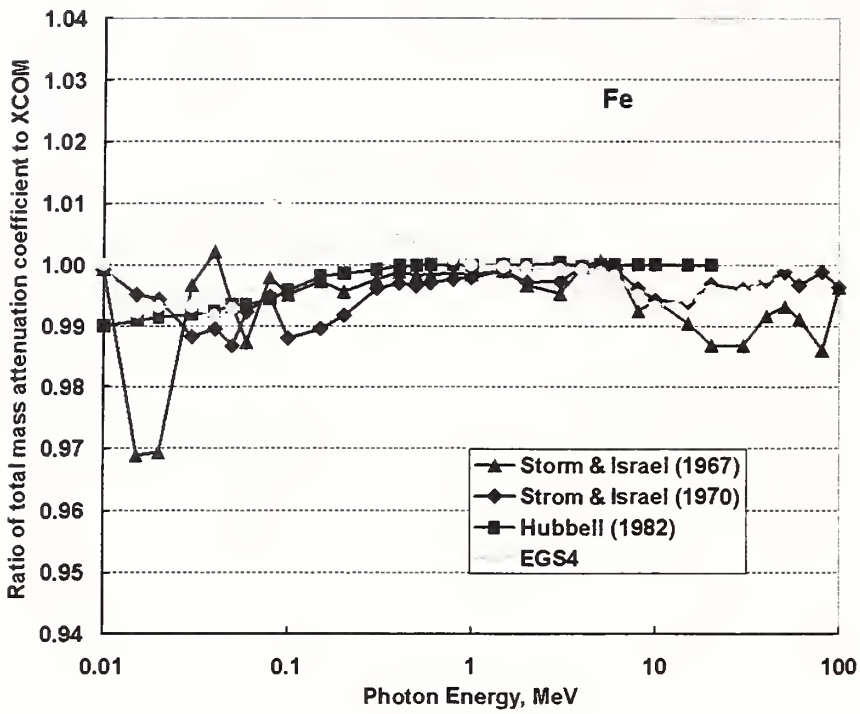

Figure 6. Ratios of total attenuation coefficients for Fe, from various tabulations, to those from the XCOM database of Berger and Hubbell (1987).

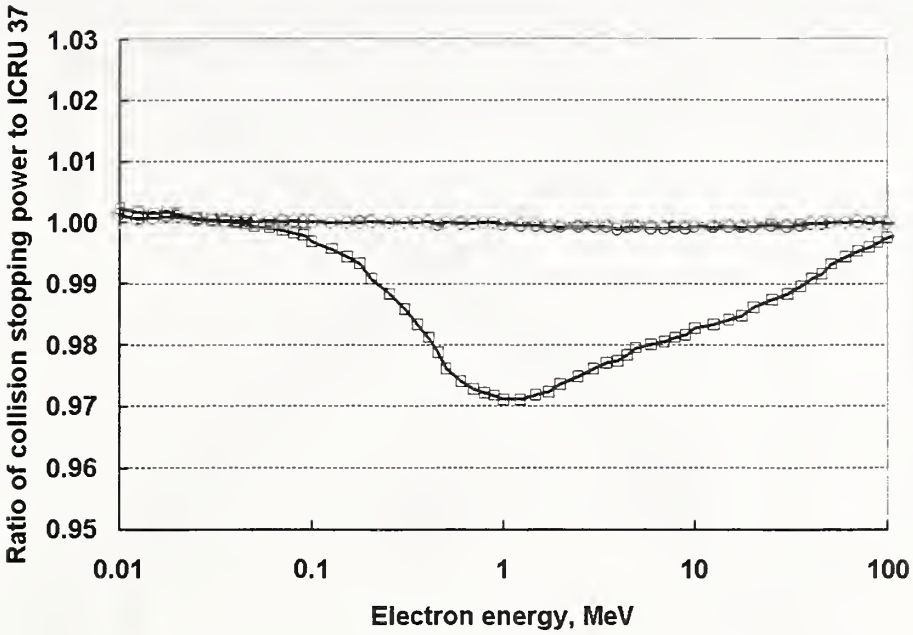

Figure 7. Ratios to that from ICRU Report 37 (ICRU, 1984) of collision stopping powers for water calculated by PENELOPE. Curve marked with circles correctly assumes water to be an insulator, and curve marked with squares inadvertently assumed it a conductor.

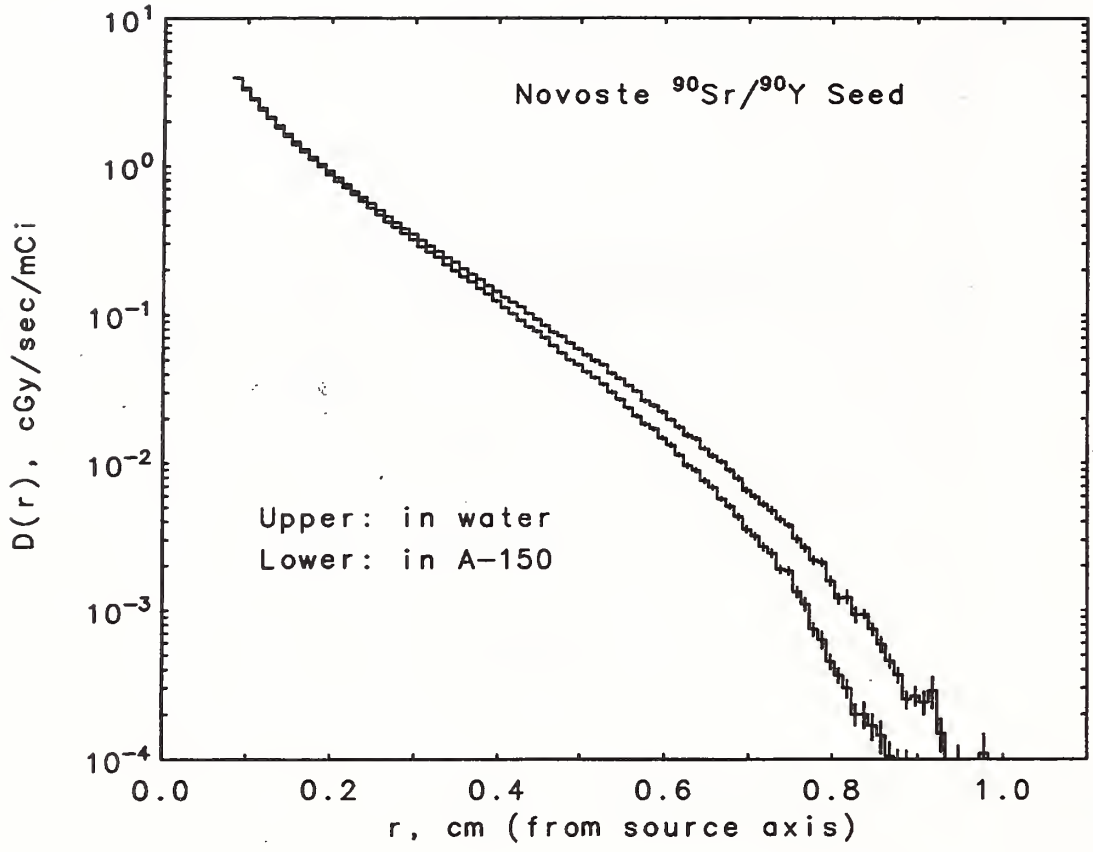

Figure 8a. Radial dose-rate distributions for the Novoste $^{90}Sr/^{90}Y$ seed, from CYLTRAN/ITS3 Monte Carlo calculations.

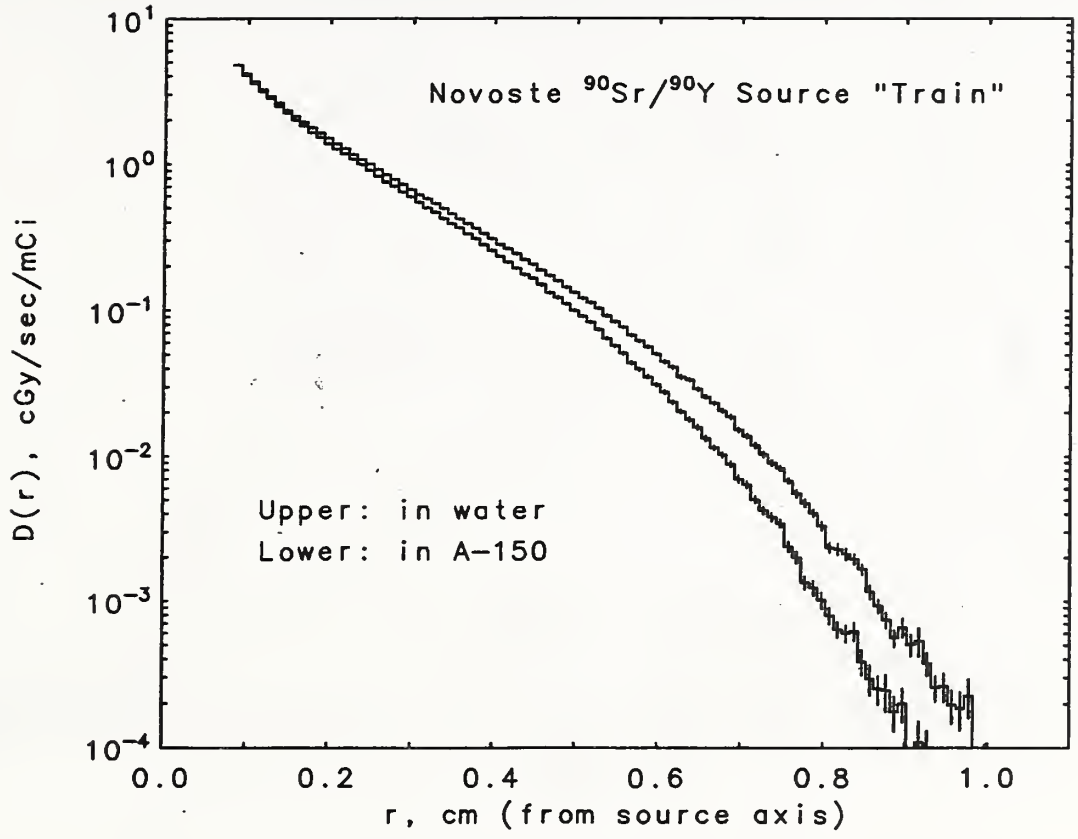

Figure 8b. Radial dose-rate distributions for the Novoste $^{90}Sr/^{90}Y$ 12-seed train, from CYLTRAN/ITS3 Monte Carlo calculations.

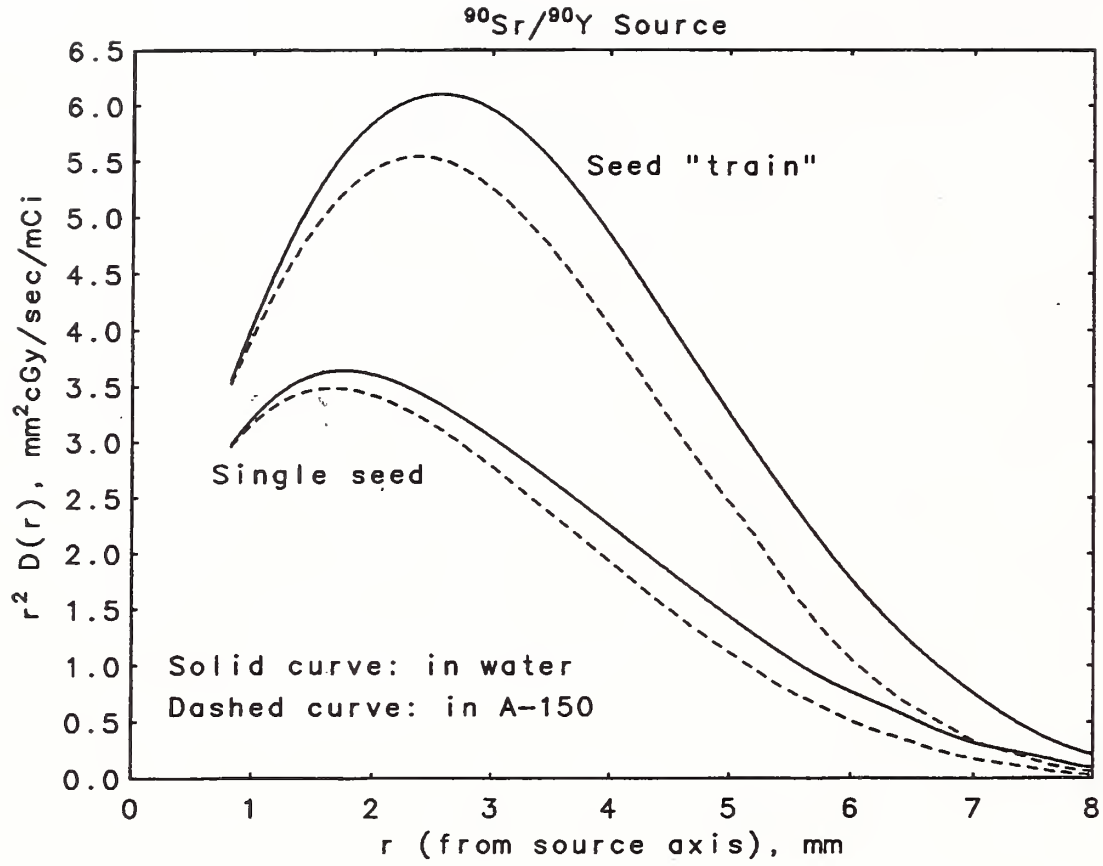

Figure 9. Radial dose-rate distributions for the Novoste $^{90}Sr/^{90}Y$ seed and train, from CYLTRAN/ITS3 Monte Carlo calculations. Note that the Monte Carlo results have been fitted with least-squares cubic splines and muliplied by the square of the radial distance.

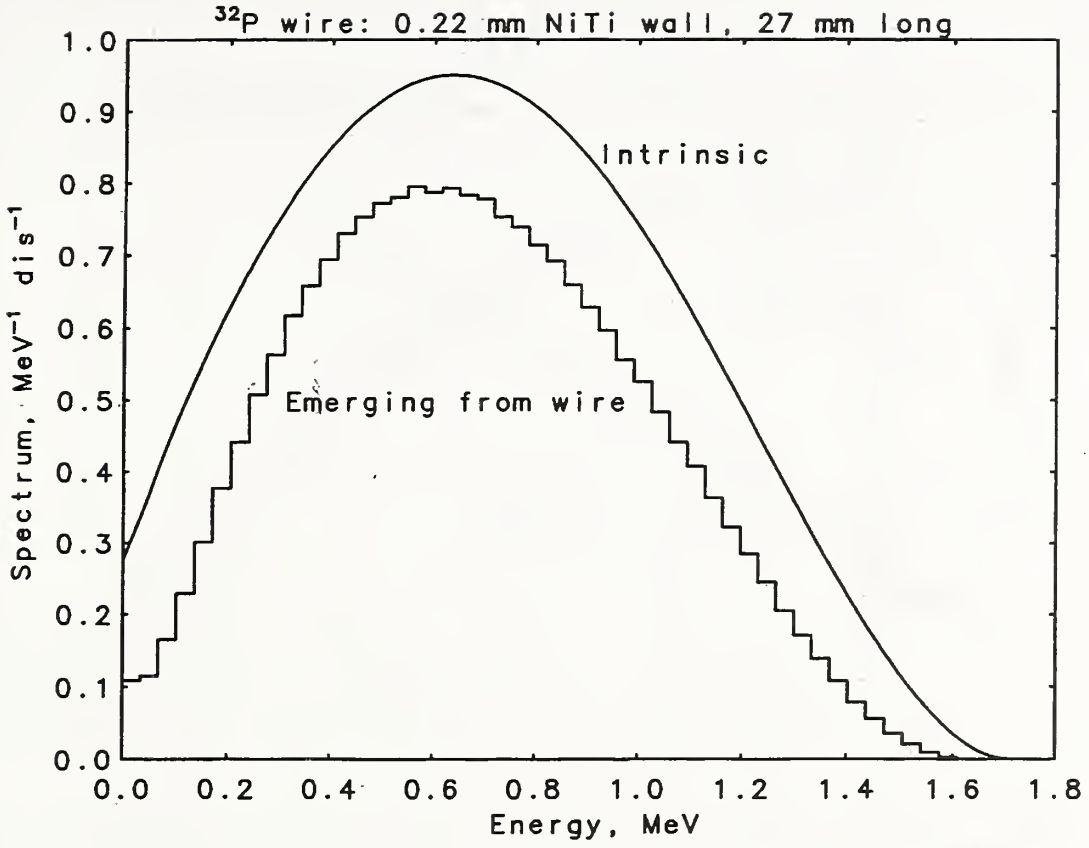

Figure 10. Comparison of the intrinsic emission spectrum of ^{32}P with the spectrum of electrons emerging from the Guidant 27 mm ^{32}P wire source. The emergent spectrum was calculated with CYLTRAN/ITS3.

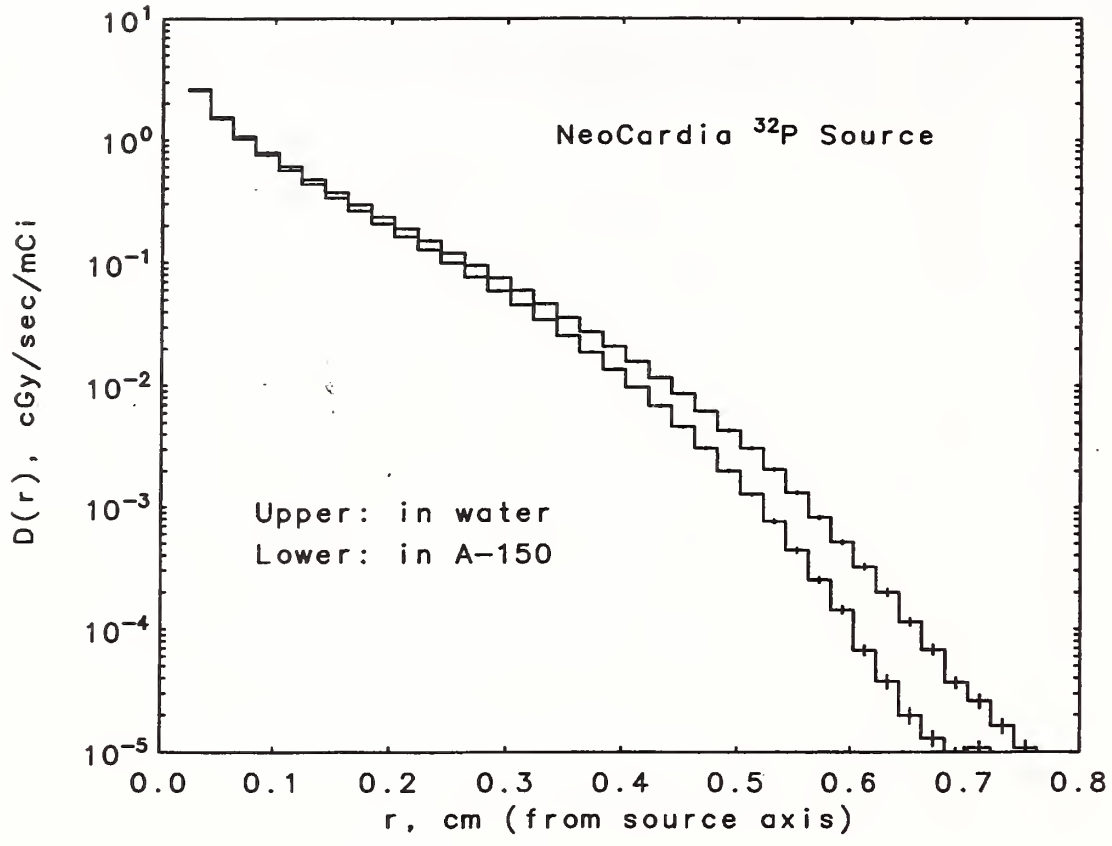

Figure 11. Radial dose-rate distributions for the Guidant 27 mm ^{32}P wire source, from CYLTRAN/ITS3 Monte Carlo calculations.

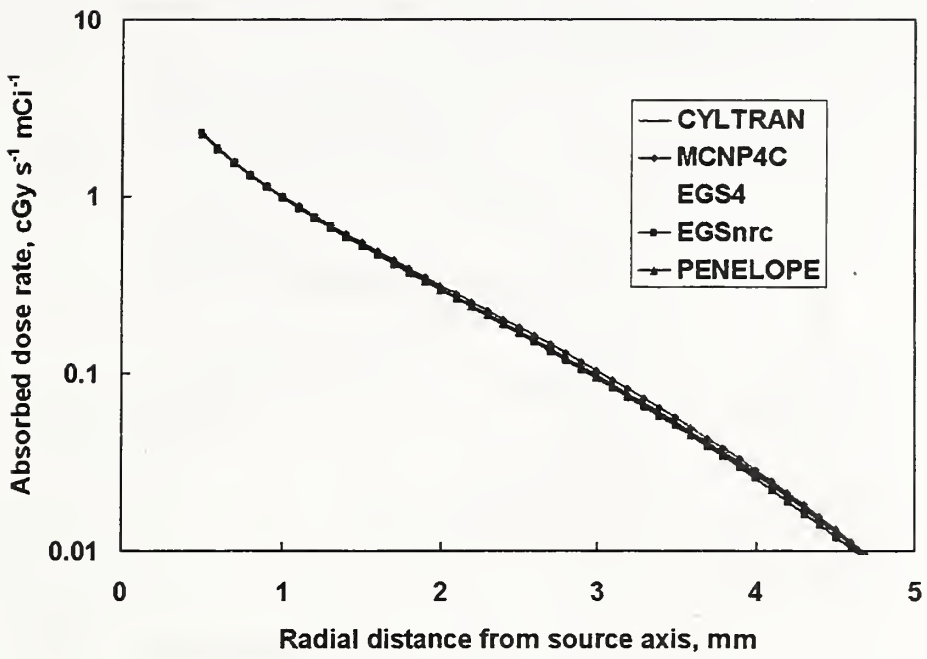

Figure 12. Radial dose-rate distributions for the Guidant 20 mm ^{32}P wire source. The results from the calculations with the various Monte Carlo codes, keeping run parameters as identical as possible, are barely distinguishable on this scale.

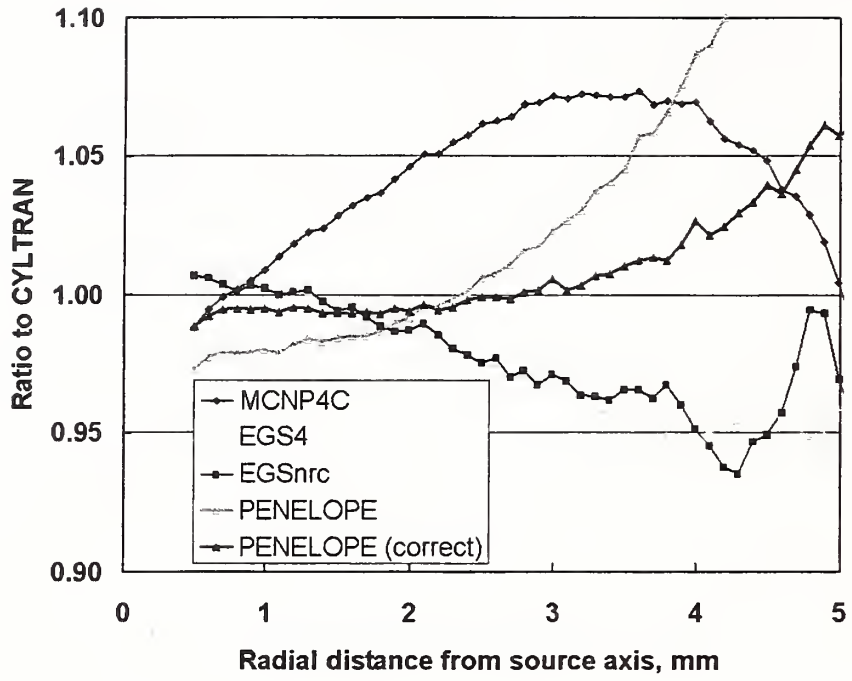

Figure 13. Ratios to the results of CYLTRAN/ITS3 of the radial dose-rate distributions calculated for the Guidant 20 mm ^{32}P wire source using the various Monte Carlo codes.

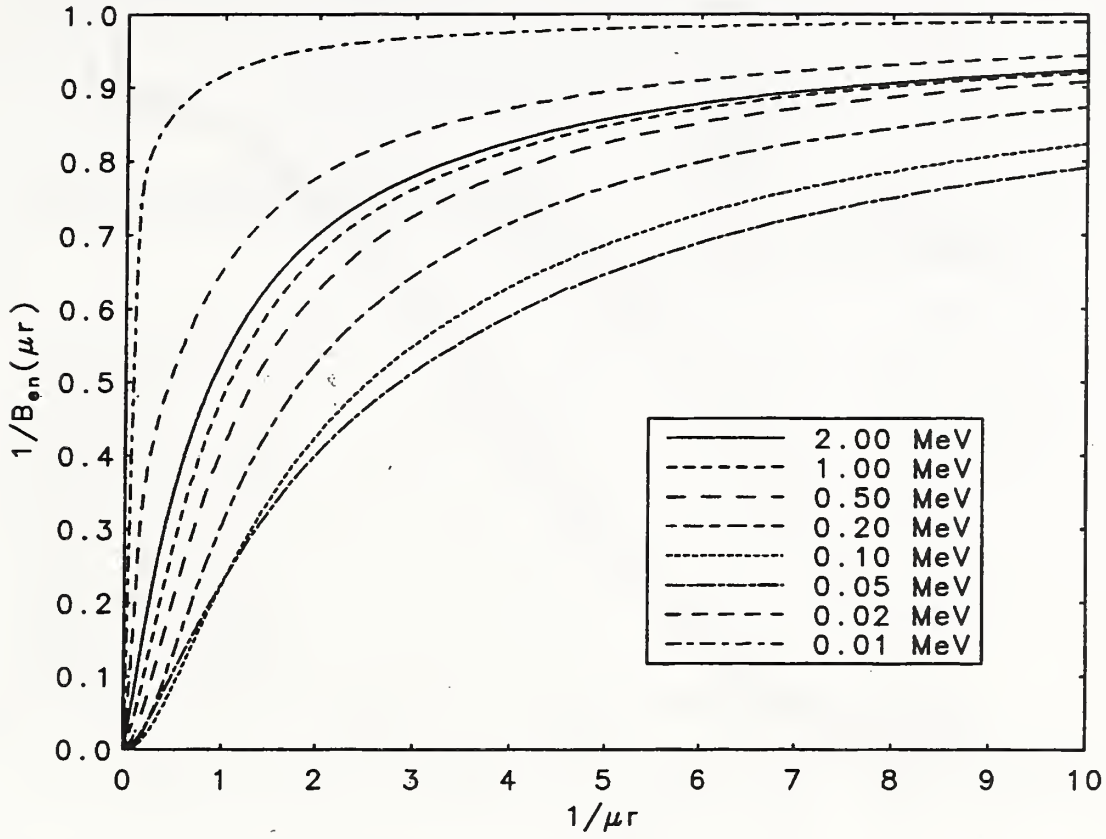

Figure 14. Energy-absorption buildup factors, $B_{en}(\mu r)$, for point-isotropic mono-energetic photon sources in water. Results out to 8 times the mean-free path, μr, were calculated directly with the ETRAN Monte Carlo code, and values for larger radii were obtained by extrapolation.

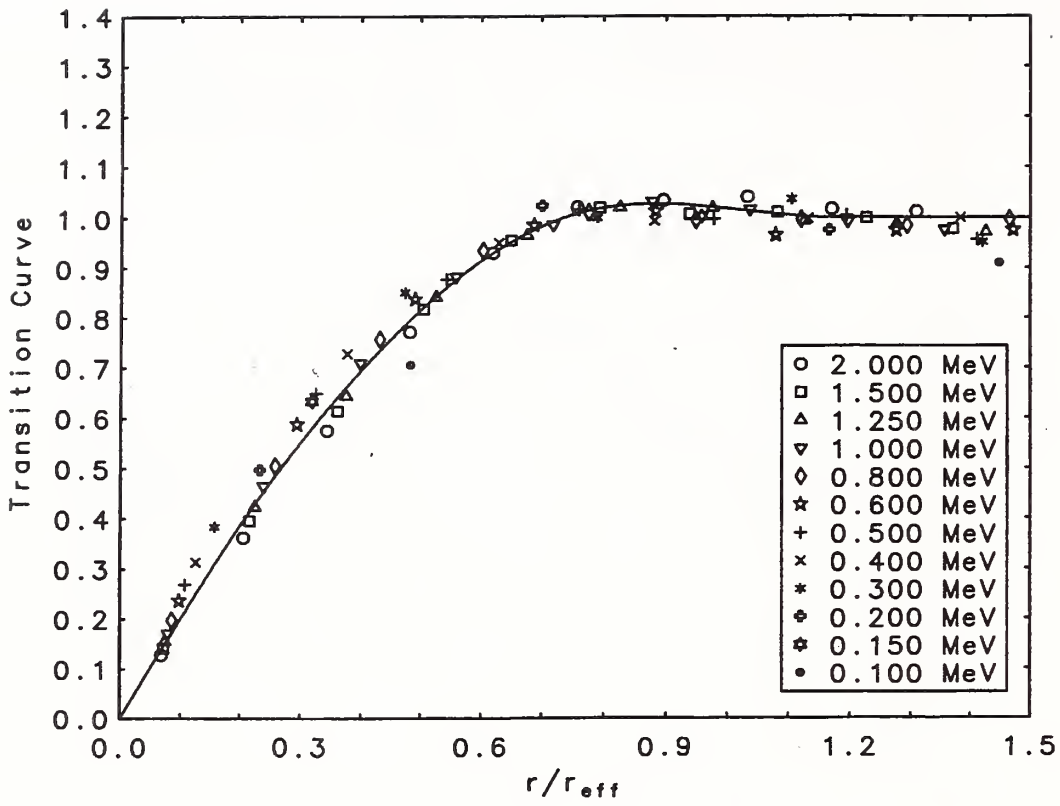

Figure 15. Universal transition function that approximates the net outward transport of secondary-electron energy for the absorbed dose from point-isotropic mono-energetic photon sources in water. Points, from ETRAN Monte Carlo calculations, are shown for various initial photon energies, and results are plotted as a function of the scaled radial distance r/r_{eff} discussed in the text.

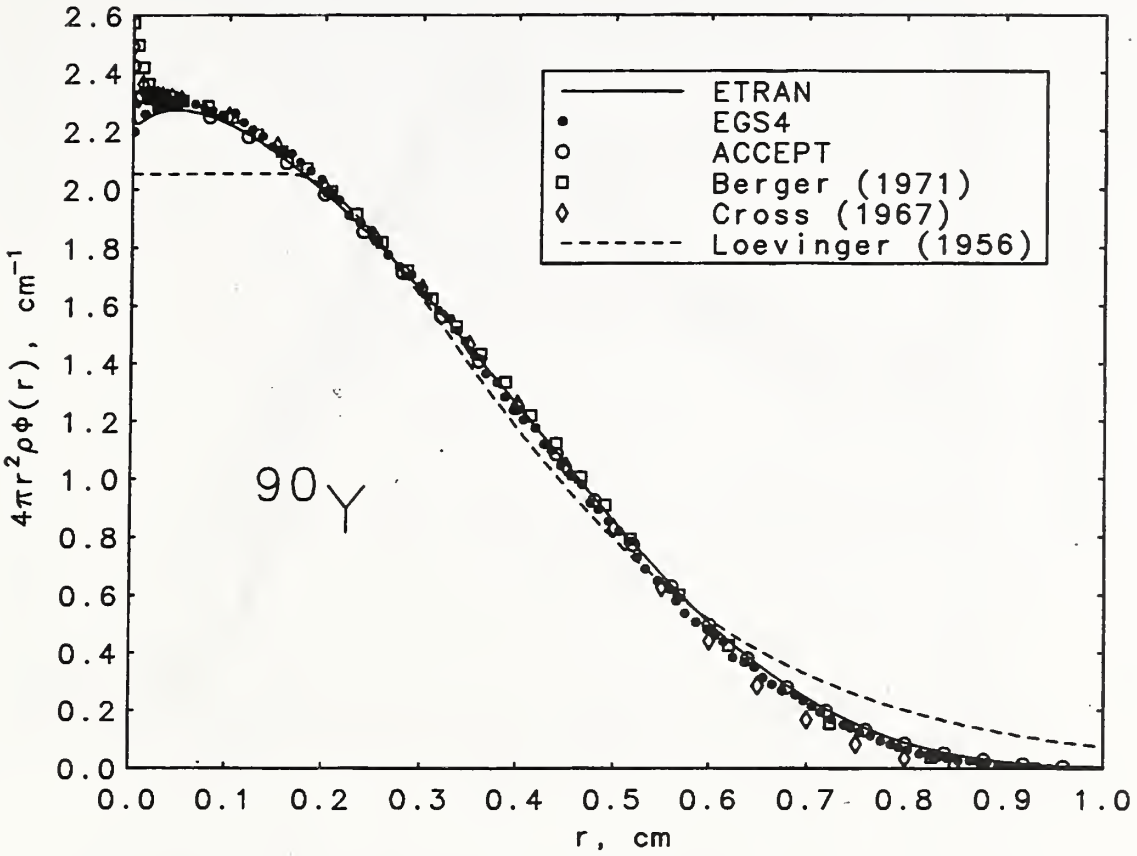

Figure 16. Scaled point kernels for the absorbed dose in an infinite water medium as a function of radial distance r from a ^{90}Y point-isotropic emitter. Results from various authors are plotted such that the areas under the curves are unity.

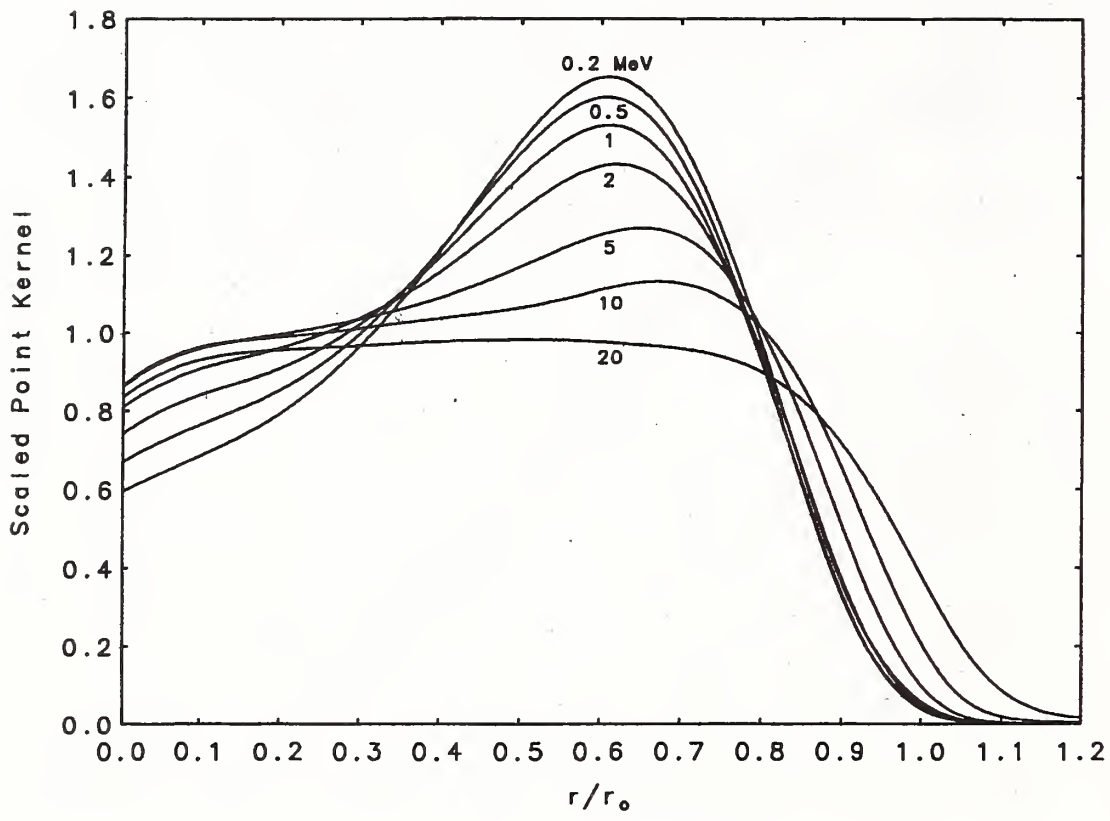

Figure 17. Scaled point kernels from ETRAN Monte Carlo calculations (Seltzer, 1991).

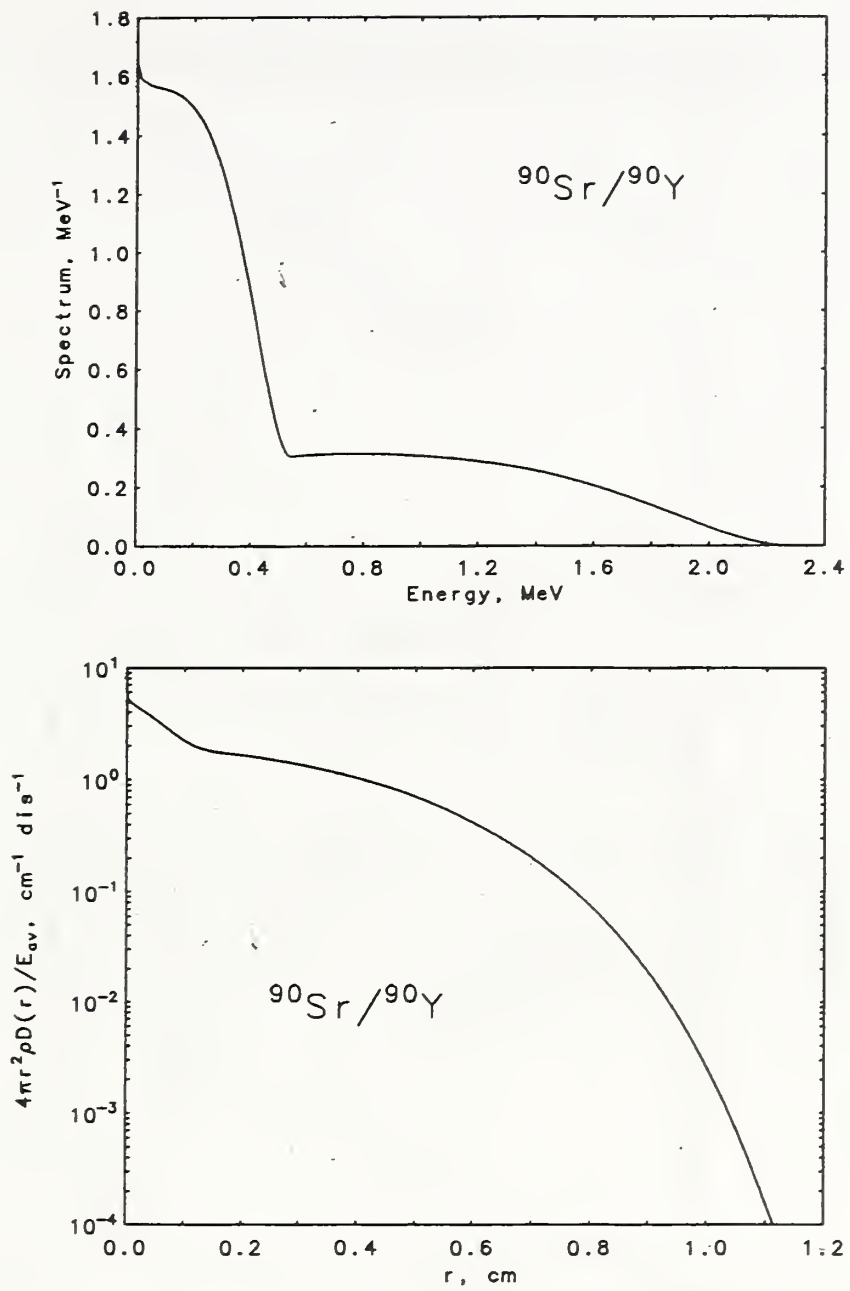

Figure 18. Intrinsic emission spectra and scaled point kernels.

a. $^{90}Sr/^{90}Y$.

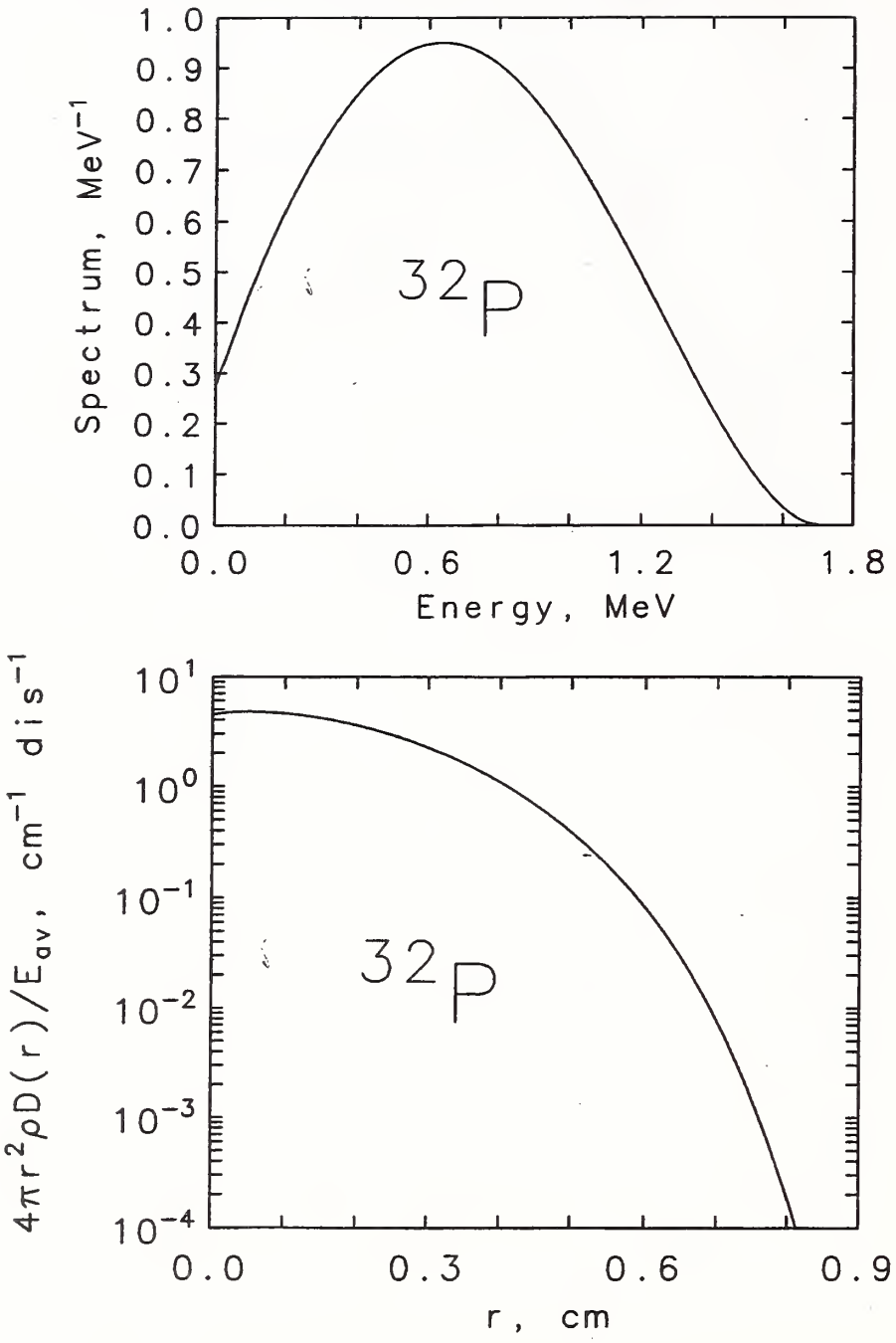

Figure 18. Intrinsic emission spectra and scaled point kernels.

b. ^{32}P.

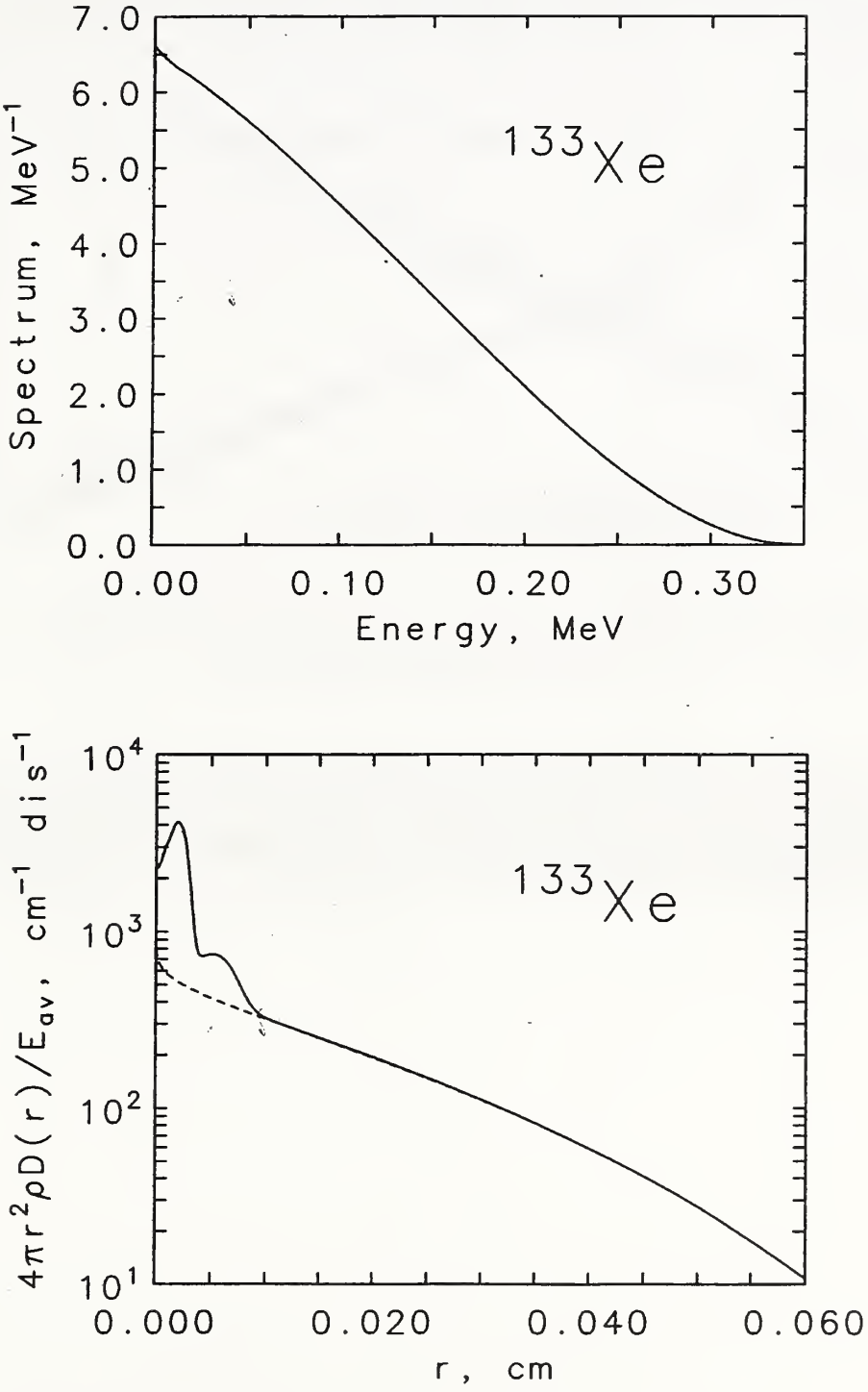

Figure 18. Intrinsic emission spectra and scaled point kernels.

c. ^{133}Xe.

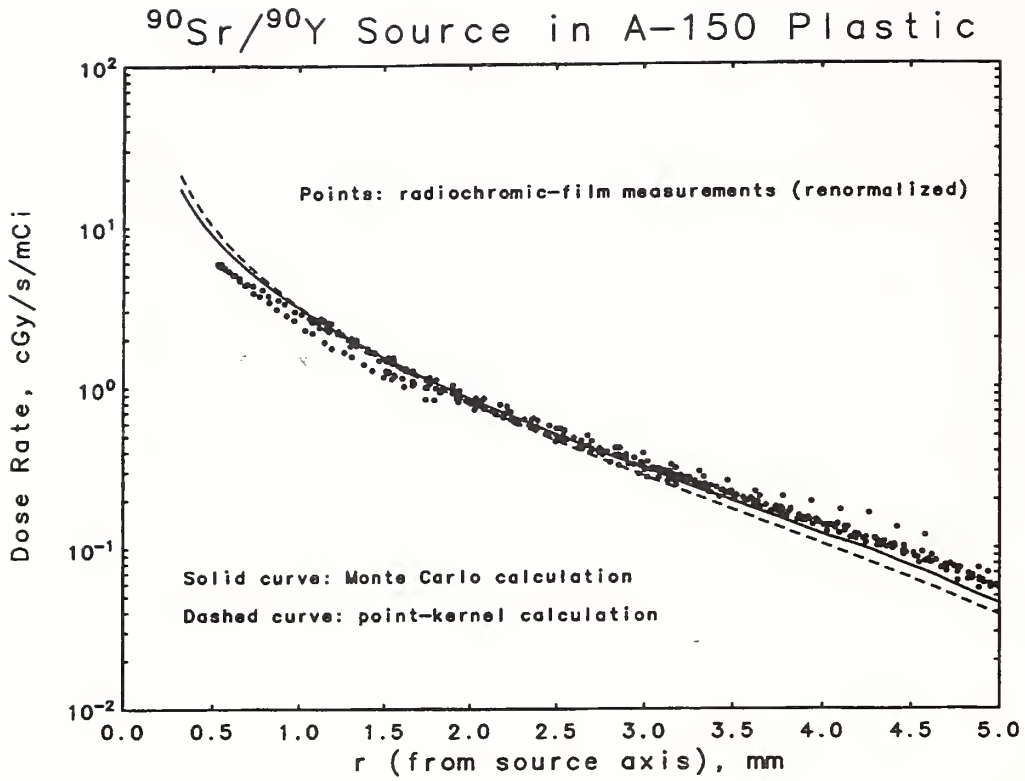

Figure 19. Comparison of the radial dose-rate distributions from Monte Carlo and from point-kernel calculations for the Novoste $^{90}Sr/^{90}Y$ seed in A-150 plastic. The Monte Carlo results are from CYLTRAN/ITS3 calculations; the measured results were provided by Chris Soares (private communication).

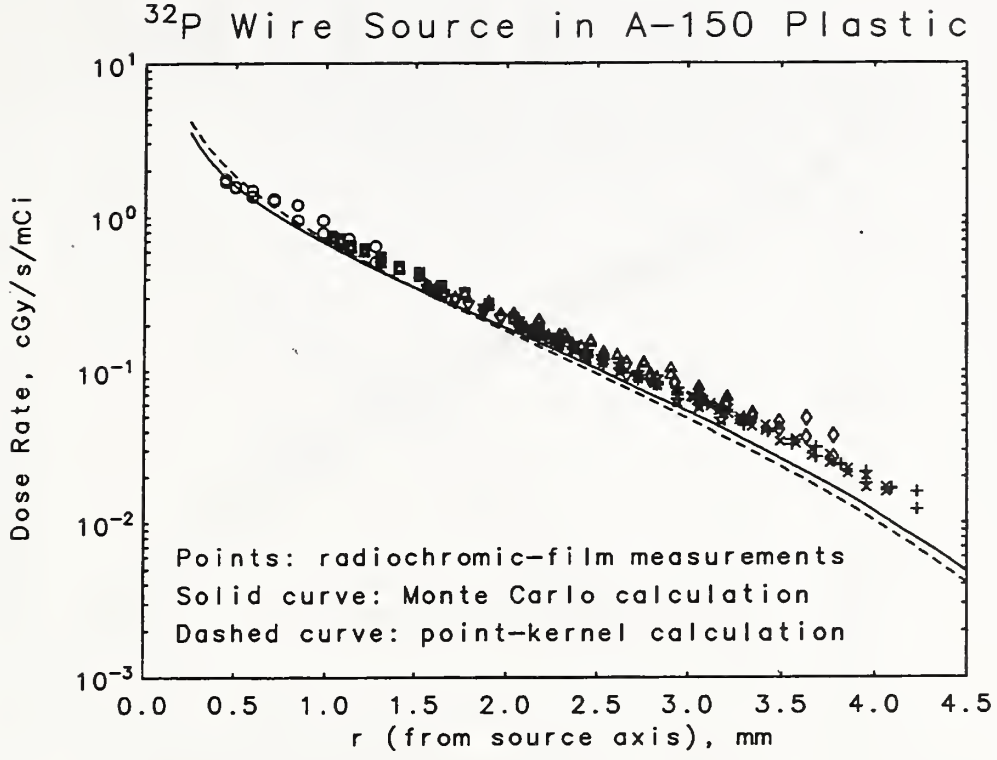

Figure 20. Comparison of the radial dose-rate distributions from Monte Carlo and from point-kernel calculations for the Guidant ^{32}P wire source in A-150 plastic. The Monte Carlo results are from CYLTRAN/ITS3 calculations; the measured results were provided by Chris Soares (private communication).

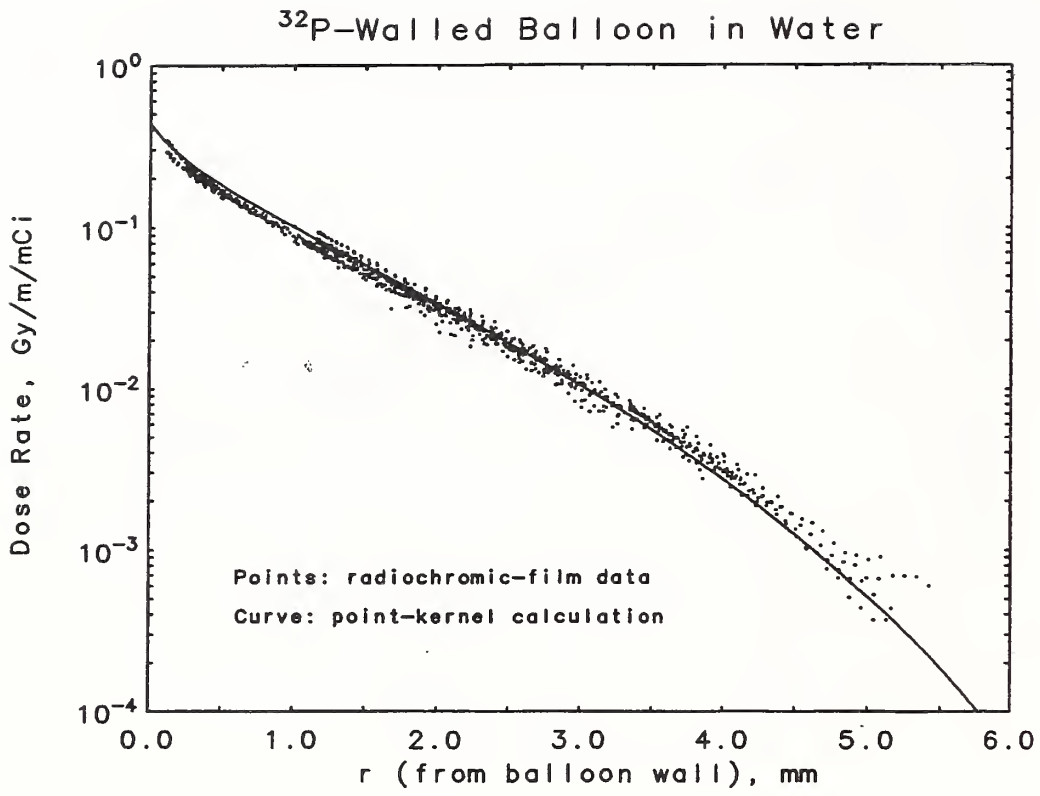

Figure 21. Comparison of the radial dose-rate distributions from point-kernel calculations and from measurements for the Radiance water-filled ^{32}P-walled balloon in a water phantom. The measured results were provided by Chris Soares (private communication).

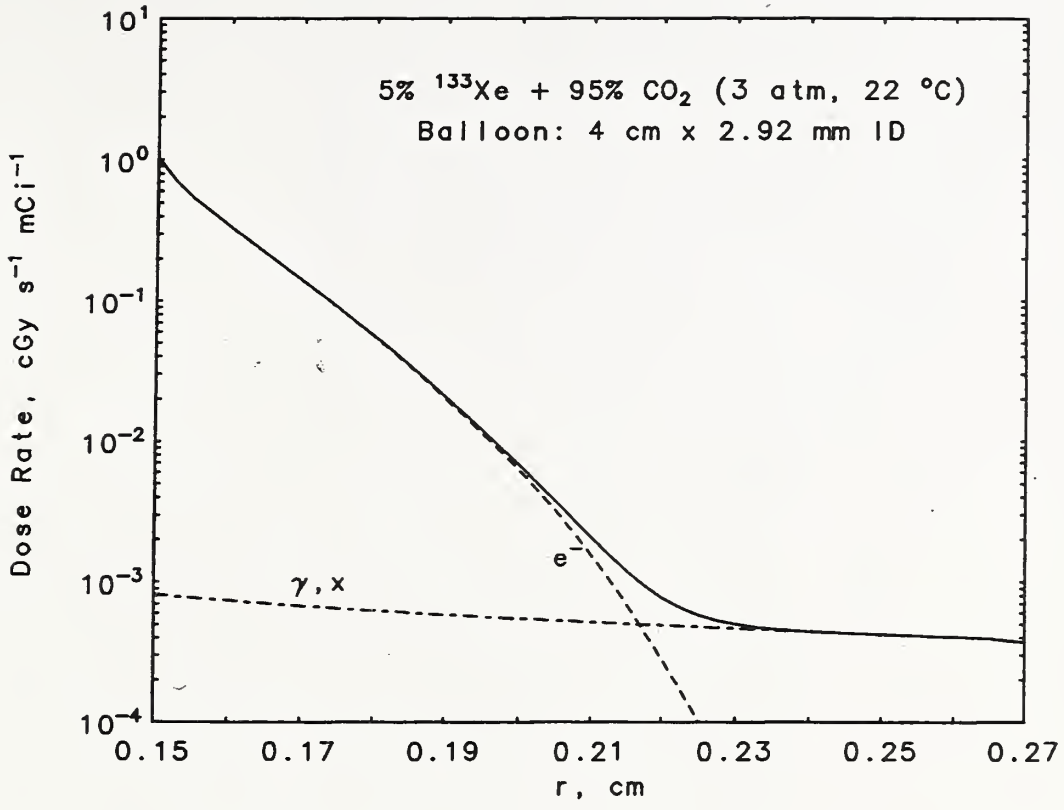

Figure 22. Radial dose-rate distributions from point-kernel calculations for a ^{133}Xe-filled balloon in water. Results, for a simple cylindrical balloon with 0.04 mm thick polyethylene walls and no central structures, are given as a function of radial distance from the source axis.